Sensitivity of Polarimetric SAR Decompositions to Soil Moisture and Vegetation Over Three Agricultural Sites Across a Latitudinal Gradient

Giovanni Anconitano, *Student Member, IEEE*, Marco Lavalle, Mario Alberto Acuña, and Nazzareno Pierdicca, *Senior Member, IEEE*

***Abstract*—The goal of this work is to assess the impact of polarimetric SAR decompositions for soil moisture retrieval, and identify the decomposition that performs best for varying vegetation covers and soil conditions. Seven polarimetric decompositions are applied to three L-band radar time-series to evaluate their relative performances for future inclusion within a soil moisture retrieval scheme. Three agricultural sites with different soil and vegetation characteristics are selected across a latitudinal gradient in America. Two time-series of quad-polarimetric data collected by the NASA/JPL Uninhabited Aerial Vehicle Synthetic Aperture Radar (UAVSAR) airborne instrument are considered for the first two sites, while quad-polarimetric images acquired by the SAOCOM-1A mission are examined for the third site. We extract a set of radar polarimetric descriptors, including the backscattering coefficients, to analyze their sensitivity to soil moisture and vegetation through correlation analysis. We also apply a simple linear regression model to each crop type and site for estimating soil moisture (or Soil Water Index) by alternatively considering a combination of the decomposition powers and of the total backscattering coefficients (γ^0, σ^0). The linear regression analysis shows that the estimates are generally comparable in terms of linear correlation and root mean square error. Results also reveal that the sensitivity of polarimetric decomposition descriptors to soil moisture and vegetation parameters depend both on crop type and area of interest, without significant differences among the various decompositions tested in this study.**

***Index Terms*—L-band, polsar, polarimetric decompositions, SAOCOM-1A, soil moisture, synthetic aperture radar, uninhabited aerial vehicle synthetic aperture radar (UAVSAR), vegetation.**

I. Introduction

MONITORING soil moisture with high spatial resolution and frequent temporal sampling is fundamental for flood forecast, drought monitoring and agricultural practices management. Synthetic Aperture Radar (SAR) data represent an important source of information for analyzing soil moisture changes over time. With the launch of the Copernicus Sentinel-1 missions, followed by the future NISAR (NASA/ISRO SAR mission) and ROSE-L missions, it is possible to address the need for monitoring field-scale soil moisture with frequent revisit time. A relevant aspect that has been analyzed so far is the fact that the radar signal is influenced not only by the dielectric properties of the soil but also by other parameters such as soil roughness, soil-vegetation interaction, and canopy structure. The combined use of forward models, such as the semiempirical Water Cloud Model (WCM), and ancillary data, including the Vegetation Water Content (VWC) and the Normalized Difference Vegetation Index (NDVI), can help disentangle the effects of vegetation from those of the soil in the radar backscattered signal [1], [2], [3]. Another possible solution is to apply polarimetric SAR decompositions to isolate scattering mechanisms (i.e., surface, double-bounce, and volume) and leverage the ones that are mostly related to soil scattering contribution. Although the importance of acquiring all polarization combinations is well established, the two approaches, i.e., using the backscattering coefficient at different polarizations corrected by auxiliary data, or removing the volume contribution using polarimetric decomposition techniques, have not been extensively compared to date. While previous works relying on specific decomposition techniques have shown that both surface and double-bounce contributions, after the volume term has been removed, can be used to estimate soil moisture with performances that depend on the crop type and the vegetation growth stage [4], [5], [6], [7], identifying the most suitable polarimetric decomposition technique remains an open question. In this work, we apply the Freeman-Durden three-components decomposition [8], the Yamaguchi four-components decomposition with rotation of the coherency matrix [9], the Singh four-components decomposition with/without extended volume scattering model [10], the Nonnegative Eigenvalue Decomposition [11], the Generalized Freeman-Durden decomposition [12], and the H\$\alpha\$ decomposition [13], [14] to different time-series of L-band quad-polarimetric radar data acquired by two different SAR sensors over three agricultural sites. The objectives of this analysis are to: 1) determine which polarimetric descriptor is mostly influenced by changes in soil moisture or vegetation;

Manuscript received 7 June 2023; revised 5 October 2023; accepted 24 October 2023. Date of publication 14 November 2023; date of current version 29 January 2024. This work was supported by Italian Space Agency through the "SAR-L: consolidamento della scienza" Project under Contract 2022-6-HH.0. *(Corresponding author: Giovanni Anconitano.)*

Giovanni Anconitano and Nazzareno Pierdicca are with the Department of Information Engineering, Electronics, and Telecommunications, Sapienza University of Rome, 00184 Rome, Italy (e-mail: giovanni.anconitano@uniroma1.it; nazzareno.pierdicca@uniroma1.it).

Marco Lavalle is with the NASA Jet Propulsion Laboratory, California Institute of Technology, Pasadena, CA 91109 USA (e-mail: marco.lavalle@jpl.nasa.gov).

Mario Alberto Acuña is with Comisión Nacional De Actividades Espaciales, Buenos Aires C1063ACH CABA, Argentina (e-mail: macuna@conae.gov.ar).

Digital Object Identifier 10.1109/JSTARS.2023.3332423

2) compare the polarimetric features against multipolarization backscattering coefficients (γ^0, σ^0) to highlight advantages and disadvantages of using polarimetric SAR decompositions; 3) evaluate which decomposition approach can be adopted within a soil moisture retrieval scheme under different soil moisture conditions and vegetation covers. To meet the study objectives, three L-band quad-polarimetric datasets have been considered. The first was collected by the NASA/JPL Uninhabited Aerial Vehicle Synthetic Aperture Radar (UAVSAR) as part of the Soil Moisture Active Passive Validation Experiment 2012 (SMAPVEX 2012) over an agricultural area South of Winnipeg (Manitoba, Canada) [15]; the second was acquired by UAVSAR during the 2019 NISAR AM/PM campaign over the Yucatan Lake region (Louisiana, USA) [16]; the third was collected by the Argentinian mission SAOCOM-1A over an agricultural region located in the Monte Buey area (Córdoba Province, Argentina).

The paper is organized as follows: Section II provides a detailed description of the three case studies and available datasets; Section III describes the methodology applied in the study; Section IV presents the study findings; Section V discusses the results and the main conclusions.

II. Study Sites and Available Datasets

Three experimental sites located across a latitudinal gradient are considered for the study. The first site is located South of Winnipeg (Manitoba, Canada), where the SMAPVEX 2012 field campaign was conducted over several crop fields [15]. The second site is an agricultural area in the Yucatan Lake region, which was selected by the NASA Jet Propulsion Laboratory for the 2019 UAVSAR AM/PM campaign. The third site is located in the agricultural region of Monte Buey, where the Argentinian Space Agency conducted a field campaign during the 2019–2020 season. Two time-series of L-band quad-polarimetric data collected by the NASA/JPL UAVSAR are analyzed for the Winnipeg and Yucatan Lake sites, respectively. UAVSAR is an L-band airborne radar with polarimetric capabilities, which collects images with a resolution of approximately 1.66m $\times$ 1m in range and azimuth, respectively, and an incidence angle varying between 25° and 65° [18]. For the Monte Buey site, a time-series of L-band quad-polarimetric data acquired by the Argentinian satellite SAOCOM-1A is considered. SAOCOM-1A is the first of a constellation of two satellites: the nominal spatial resolution of the quad-polarimetric L1A products (Single Look Complex), acquired in STRIPMAP mode, is 10m $\times$ 6m in ground range and azimuth, respectively, while the revisit time is equal to sixteen days; considering all the ten subswaths, the minimum incidence angle range varies between 17.6° and 35.5° [19]. A detailed description of the three sites and related datasets is reported in the following sections.

A. Winnipeg Site: SMAPVEX 2012 Campaign

The experiment took place over an agricultural area located south of Winnipeg (Manitoba, Canada) between 7 June and 19 July 2012 to collect both airborne and ground data to be used for developing and testing the Soil Moisture Active Passive (SMAP) soil moisture retrieval algorithms [15]. Experimental data are made available freely by the investigators of the SMAPVEX 2012 at [17]. In this paper, fourteen Single Look Complex (SLC) L-band products acquired during the UAVSAR flight line number 31605 were selected, as reported in Table I.

TABLE I
SMAPVEX 2012 UAVSAR Acquisitions

Flights	Days	Flights	Days
12044	17-06-2012	12055	03-07-2012
12045	19-06-2012	12056	05-072012
12046	22-06-2012	12057	08-07-2012
12047	23-06-2012	12058	10-07-2012
12048	25-06-2012	12059	13-07-2012
12049	27-06-2012	12060	14-07-2012
12050	29-06-2012	12061	17-07-2012

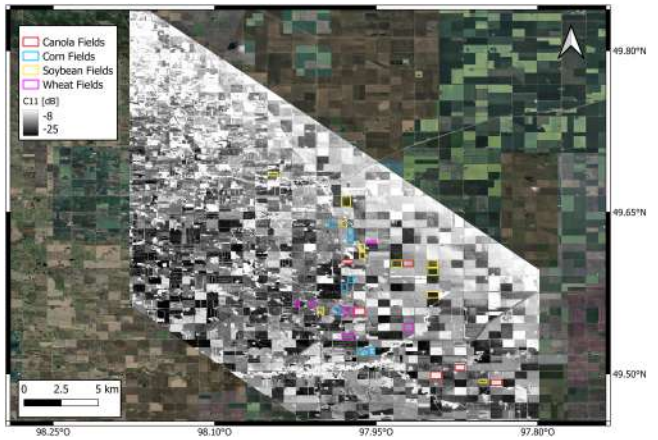

Fig. 1. Winnipeg study site. The C11 element (dB) of the covariance matrix extracted from the first UAVSAR acquisition (17-06-2012) is shown along with the thirty-one crop fields considered for the analysis, which are displayed according to their crop type (red: canola; light blue: corn; yellow: soybean; purple: wheat).

During the field campaign, soil and vegetation parameters, such as soil moisture, surface roughness, and biomass were collected for 55 crop fields. As for the soil moisture, it was measured at sixteen sampling points for each agricultural field, with three replicated measurements at each sampling point. In this work, the mean soil moisture value obtained by averaging the sixteen measurements is used as reference value for each field. We selected thirty-one crop fields: 11 soybeans, 6 wheat, 6 canola, and 8 corn. Fig. 1 shows the area of interest along with the element (1, 1), or C11, of the polarimetric covariance matrix extracted from the first UAVSAR acquisition (17-06-2012); the thirty-one crop fields considered in the study are also displayed according to their crop type (red: canola; light blue: corn; yellow: soybean; purple: wheat).

B. Yucatan Lake Site: 2019 NISAR AM/PM Campaign

The 2019 NISAR UAVSAR AM-PM campaign was conducted in the South-Eastern United States to collect data for guiding the development of the NISAR ecosystem science algorithms [16]. For the analysis in this paper, thirteen SLC L-band UAVSAR images acquired between June and October 2019 over

TABLE II
2019 UAVSAR NISAR AM/PM CAMPAIGN ACQUISITIONS

AM Flights	Days	PM Flights	Days
19043	01-07-2019	19040	22-06-2019
19048	16-07-2019	19044	03-07-2019
19051	25-07-2019	19049	18-07-2019
19053	12-08-2019	19052	27-07-2019
19069	23-09-2019	19054	14-08-2019
19070	30-09-2019	19071	02-10-2019
		19078	16-10-2019

Fig. 2. Yucatan lake study site. The C11 element (dB) of the covariance matrix extracted from the first AM UAVSAR acquisition (01-07-2019) is displayed along with the seven crop fields considered for the analysis (red).

an agricultural region near the city of St. Joseph in the Yucatan Lake region (Louisiana, USA) were considered, as reported in Table II.

Seven regions of interest (i.e., crop fields) were selected; their NDVI was extracted from the Sentinel-2 optical data and linearly interpolated at the UAVSAR acquisition days. Since soil moisture measurements were not available over this site, the Soil Water Index (SWI) provided by the C-band ASCAT sensor onboard the Metop satellites and distributed by the Copernicus Global Land Service was used to perform the analysis [20]: we selected the daily SWI products at global scale with a T-value equal to 1 and a resolution of 12.5 km; the T-value quantifies the influence of surface soil moisture observations taken in the past on the current SWI [21]. Fig. 2 shows the site of interest along with the element (1, 1) of the polarimetric covariance matrix extracted from the first AM UAVSAR acquisition (01-07-2019); the seven crop fields considered in the analysis are also displayed in red.

C. Monte Buey Site: 2019–2020 CONAE Field Campaign

The campaign took place during the 2019–2020 growing season over an agricultural region in the Monte Buey area (Córdoba Province, Argentina); it was conducted by the Comisión Nacional De Actividades Espaciales (CONAE) to collect ground data, such as soil moisture, plant height, and growth stage

TABLE III
2019–2020 FIELD CAMPAIGN SAOCOM-1A ACQUISITIONS

Days		
13-10-2019	30-11-2019	17-01-2020
29-10-2019	16-12-2019	02-02-2020
14-11-2019	01-01-2020	18-02-2020

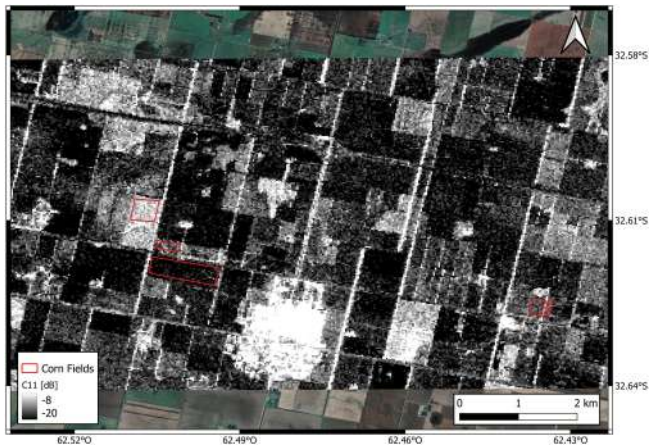

Fig. 3. Monte Buey study site. The C11 element (dB) of the covariance matrix extracted from the first SAOCOM acquisition (13-10-2019) is displayed along with the five corn fields considered for the analysis (red).

concurrently with the SAOCOM-1A overpasses. The area is a validation site of the NASA SMAP mission, and it is also used to validate the soil moisture products generated by CONAE from SAOCOM data. In this study, a time-series of nine L-band SLC STRIPMAP images acquired along descending orbits between 13 October 2019 and 18 February 2020 was selected with a revisit time of sixteen days, as reported in Table III.

The analysis was carried out considering five corn fields. The NDVI for each field was calculated from the Sentinel-2 optical data and linearly interpolated at the time of SAOCOM overpasses. Fig. 3 shows the area of interest along with the element (1, 1) of the polarimetric covariance matrix extracted from the first SAOCOM acquisition (13-10-2019); the five corn fields are also displayed in red.

III. METHODOLOGY

A. Polarimetric SAR Decompositions

Denoting with $\boldsymbol{S}$ the complex scattering matrix measured by a radar polarimeter (with elements S_{HH}, S_{HV}, S_{VH}, and S_{VV}), the 3×3 polarimetric covariance or coherency matrices (C3/T3) were generated for each site of interest by forcing $S_{\mathrm{HV}} = S_{\mathrm{VH}}$ [22]. Seven polarimetric decompositions were considered for this study: Freeman-Durden three-components (FD) [8], Yamaguchi four-components with rotation of the coherency matrix (Y4R) [9], Singh general four-components with unitary transformation of the coherency matrix with/without extended volume scattering model (G4U2/G4U1) [10], Nonnegative Eigenvalue Decomposition (NNED) [11], the Generalized Freeman-Durden Decomposition (FDG) [12], and the H/α decomposition [13],

[14]. A summary of the main features and differences between these decomposition approaches is reported below, whereas the detailed mathematical description can be found in [8], [9], [10], [11], [12], [13], and [14]. The Freeman-Durden three-components decomposition separates the measured covariance matrix C3 into three statistical uncorrelated contributions: surface, double-bounce, and volume scattering.. The surface term is modeled by a first-order Bragg model; the double-bounce contribution, describing, for example, the interaction between ground and trunks in a forest, is modeled as a dihedral corner reflector with the two reflecting surfaces that can be characterized by different dielectric properties; the volume term models the canopy layers as a cloud of randomly oriented, very thin, cylinder-like scatterers. The Yamaguchi four-components decomposition with rotation of the coherency matrix is based on the original Yamaguchi four-components algorithm described in [23], which extends the three-components approach proposed by Freeman-Durden by adding a fourth term to the surface, double bounce, and volume contributions. This term is called helix scattering term and it accounts for the correlation between the copolarizations and the cross-polarizations, which appears in complex urban areas and disappears for almost all natural distributed scatterers; this condition corresponds to have $\langle S_{\mathrm{HH}} S_{\mathrm{HV}}^{*} \rangle \neq 0$ and $\langle S_{\mathrm{VV}} S_{\mathrm{HV}}^{*} \rangle \neq 0$, which is equal to a non-reflection symmetry condition. In addition, the volume term is modified according to the relative magnitude of $\langle |S_{\mathrm{HH}}|^2 \rangle$ versus $\langle |S_{\mathrm{VV}}|^2 \rangle$ by introducing a probability function that accounts for the orientation angle distribution of the dipoles, which in the FD scheme are assumed to be randomly oriented. The Y4R introduces a rotation of the coherency matrix to minimize the cross-polarized component and then applies the original four-components algorithm described in [23]. In 2013, Singh proposed a general four-components decomposition by introducing an additional special unitary transformation of the rotated coherency matrix. The algorithm also provides the use of an extended volume scattering model to better discriminate the volume scattering between dipoles and dihedral scattering structures caused by the HV component [10]. We considered two versions of this decomposition, G4U2 and G4U1, with and without the extended volume model, respectively. A possible shortcoming of the Freeman-Durden and Yamaguchi approaches is that some pixels of the scattering mechanisms (i.e., the power associated to a scattering mechanism) may have negative values, which represent a nonphysical result. To overcome this issue, van Zyl and Kim proposed a new technique called Nonnegative Eigenvalue Decomposition [11]. The main hypothesis of the NNED is that the eigenvalues of the remainder matrix, obtained after removing the volume term from the measured covariance matrix, are real and greater than or equal to zero. This result can be achieved by adequately modeling the canopy scattering; then, an eigenvector decomposition is applied to the remainder matrix allowing to associate the eigenvectors to surface and double-bounce contributions. The Generalized Freeman-Durden decomposition, as described in [12], postulates that the surface and double-bounce contributions are orthogonal: this reduces by one the parameters that need to be estimated. The parameters of the decomposition are then calculated by applying an eigenvalue/eigenvector decomposition, which also ensures non-negative powers. In general, it is possible to assume that the contribution of each scattering mechanism to the total power P_t can be split among scattered power terms P_s, P_d, and P_v, which correspond to surface, double-bounce, and volume powers, respectively

$$P_t = P_s \ + P_d + P_v. \tag{1}$$

The H/α decomposition relies on a eigenvalues/eigenvectors analysis of the covariance or coherency matrix from which the entropy H and the alpha angle α descriptors are derived [13], [14]. The entropy is obtained from the eigenvalues of the polarimetric matrices C3/T3; it is a measure of target randomness, and it varies between 0 (single, nonrandom targets) and 1 (random targets). The alpha angle is obtained from the eigenvectors of the polarimetric matrices C3/T3, and it is the main parameter used to identify the mean dominant scattering mechanism. Values of alpha in the range 0° to approximately 40° correspond to surface scattering; values of alpha in the approximate range of 40°–50° correspond to volume scattering; and values of alpha in the approximate range of 50° to 90° indicate double-bounce scattering.

B. SAR Data Preparation and Processing

The SLC UAVSAR and SAOCOM-1A images acquired over the three sites of interest were processed by following multiple steps to generate a stack of geocoded and coregistered polarimetric C3/T3 matrices. For SMAPVEX 2012, the SLC images were multilooked by using an adaptive algorithm to obtain a final pixel spacing of the C3/T3 matrices of 15m × 15m in latitude and longitude, respectively, which corresponds to an average number of looks of about 160. Then, an algorithm for radiometric terrain correction was applied to calibrate the polarimetric matrices to gamma-naught (γ^0) [24]. The same steps were replicated for the Yucatan Lake site. In this case, the SLC images were multilooked by an adaptive number of looks that is different for the AM and PM flights since the direction of the two flights is different. The final pixel spacing of the C3/T3 matrices is 20m × 20m in latitude and longitude, respectively, which corresponds to a number of looks ranging between 180 and 330. Then, the previous algorithm for radiometric terrain correction was applied to calibrate the matrices to gamma-naught. For the Monte Buey site, the SLC products, already calibrated to sigma-naught (σ^0), were multilooked by 18 looks (3×6 in range and azimuth). The polarimetric C3/T3 matrices were then terrain corrected, geocoded, and resampled to 30m × 30m. The result of the processing workflows is a set of three time-series of polarimetric C3/T3 matrices to which the seven polarimetric decompositions described in Subsection III-A were applied. We recall that the main objective of the work is to separate scattering mechanisms and evaluate which polarimetric descriptors are mostly influenced by changes in soil moisture and vegetation, also compared to the multipolarization backscattering coefficient. Therefore, different sets of descriptors, reported in Table IV, were investigated and compared by a statistical analysis.

The backscattering coefficient sigma-naught (σ^0) or gamma-naught (γ^0) at different polarizations (HH, HV, VV), the SPAN,

TABLE IV
TOTAL AND POLARIMETRIC DESCRIPTORS EXTRACTED OVER THE THREE SITES OF INTEREST

Descriptors	
$\gamma^0_{HH}, \gamma^0_{HV}, \gamma^0_{VV}$	Backscattering coefficient (dB) - SMAPVEX 2012, Yucatan Lake
$\sigma^0_{HH}, \sigma^0_{HV}, \sigma^0_{VV}$	Backscattering coefficient (dB) - Monte Buey
$SPAN$	Total backscattered power (dB)
HH/VV	Total co-polarization ratio (dB)
P_s	Surface power (dB)
P_d	Double-bounce power (dB)
P_v	Volume power (dB)
H	Polarimetric entropy
α	Polarimetric alpha angle (deg)

which is given by the sum of the elements on the main diagonal of C3/T3, and the copolarization ratio of HH to VV were extracted from the measured polarimetric covariance matrix before applying the decompositions: they are referred to as *total descriptors*. The *polarimetric descriptors* (surface power, double-bounce power, volume power, H, and α) were obtained after the application of the polarimetric decompositions. For the three sites of interest and each SAR time-series, the mean value of the descriptors reported in Table IV were calculated at field-level by averaging all pixels within each region of interest (i.e., crop fields). The boundaries of the crop fields in the SMAPVEX 2012 dataset were provided as shapefiles, but a manual identification was done in all cases to disregard pixels that were visibly not representative of the fields (e.g., bright targets associated with man-made structures). For SMAPVEX 2012 and Monte Buey, the calculated mean values for each field were aggregated according to their crop type and analyzed over time to investigate the dependency of both total and polarimetric descriptors on soil moisture and vegetation variations.

C. Statistical Analysis and Linear Regression Model

A statistical analysis was carried out for the three sites of interest to evaluate the correlation between the different descriptors, both total and polarimetric, and the measured target variables (soil moisture, SWI, plant biomass, plant height, and NDVI). As it will be presented later, different figures of merit were used to perform this statistical analysis: the Pearson linear correlation coefficients, the Spearman's rank correlation coefficients, the root mean square error, and the significance coefficient. The Pearson linear correlation coefficients (r) and the Spearman's rank correlation coefficients (ρ) were calculated for all the descriptors. The Pearson's correlation is a measure of the linearity of the relationship between two variables. The Spearman's correlation describes the relationship between two parameters by using a monotonic function, whether linear or not. The purpose of using both Pearson and Spearman correlation metrics is to offer a deeper interpretation of the correlation between descriptors and in-situ variables. Some descriptors may be correlated with in-situ variables through a nonlinear relationship. The obtained values were then compared among each other to evaluate the sensitivity of the descriptors to soil and vegetation data. For each crop type of SMAPVEX 2012 and the corn fields of Monte Buey a simple linear regression model was also applied to estimate soil moisture (SM) by using (2) and (3), which consider alternatively as predictors the backscatter coefficients gamma-naught or sigma-naught (expressed in dB) at different polarizations (2) or the surface P_s, double-bounce P_d, and volume P_v powers (expressed in dB) obtained after applying the polarimetric SAR decompositions (3). Due to the unavailability of in-situ soil moisture and crop type data in Yucatan Lake, (2) and (3) were used to predict the Soil Water Index instead of soil moisture, combining all the selected fields

$$\mathrm{SM} = a_1 + a_2 p^0_{\mathrm{HH}} + a_3 p^0_{\mathrm{HV}} + a_4 p^0_{\mathrm{VV}} \tag{2}$$

$$\mathrm{SM} = a_1 + a_2 P_s + a_3 P_d + a_4 P_v \tag{3}$$

where a_1, a_2, a_3, and a_4 are the coefficients to be estimated from the data and p^0_{pq} are either the gamma-naught γ^0_{pq} for SMAPVEX 2012 and Yucatan Lake, or the sigma-naught σ^0_{pq} for Monte Buey. The mean value of the descriptors (gamma-naught or sigma-naught, the powers derived from polarimetric decompositions, and the in-situ soil moisture measurements or the Soil Water Index) calculated at field-level are used as training and test sets; soil moisture or Soil Water Index are the parameters to be estimated. In this context, the performances offered by the two linear models are evaluated without separating the training set from the test set. The exercise was intended to preliminary analyze the retrieval performance using a single scattering mechanism or a combination of the three contributions (surface, double-bounce, and volume) as compared to the retrieval performance offered by the multipolarization backscattering coefficient in different combinations. The two simple linear regression models represent, along with the correlation analysis, an additional tool for comparing the capability of different sets of descriptors to predict soil moisture. They were selected in accordance with the fact that the relationship between soil backscatter and soil moisture is linear, as also reported in [25]. In Section IV, the results of this exercise are reported in terms of Pearson linear correlation between the measured and estimated soil moisture values (Soil Water Index for the Yucatan Lake site), and root mean square error (RMSE), which is given by

$$\mathrm{RMSE} = \sqrt{\frac{\sum_{i=1}^{N} \left(\widehat{\mathrm{SM}}_i - \mathrm{SM}_i\right)^2}{N}} \tag{4}$$

where $\widehat{\mathrm{SM}}_i$ and SM_i are, respectively, the estimated and measured soil moisture (Soil Water Index for the Yucatan Lake site) values, and N is the number of samples. The significance coefficient (p-value) is also used for evaluating the two regression models: it determines whether the results are statistically significant or not. Finally, Fig. 4 summarizes the steps that have been taken to accomplish the objectives of this study. The blue boxes contain the input datasets (SAR images and field data), as described in Section II; the yellow box refers to the preprocessing that allow to extract the geocoded polarimetric C3/T3 matrices; the green box contains the seven polarimetric SAR decompositions that are applied to the polarimetric matrices in

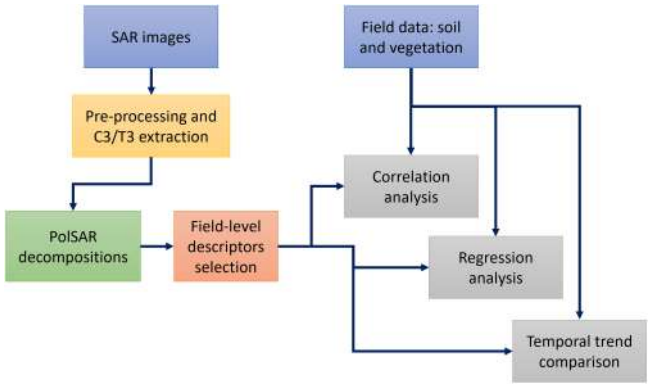

Fig. 4. Schematic flowchart of the steps that have been followed for the analysis. Blue boxes represent the input datasets, yellow box contains the preprocessing steps and the C3/T3 extraction, the green box represents the application of the seven polarimetric SAR decompositions, orange box refers to the selection of different descriptors at field-level, and gray boxes are the core part of the analysis (correlation analysis, regression analysis, and temporal trend comparison).

order to extract at field-level the different descriptors described in Table IV (orange box); finally, the gray boxes represent the core part of the study: correlation analysis, regression analysis, and temporal trend comparison.

IV. Results

In this section, the study findings are reported for the three experimental sites that have been considered: Winnipeg site - SMAPVEX 2012 Campaign (*A*), Yucatan Lake site - 2019 NISAR AM/PM Campaign (*B*), and Monte Buey site - 2019–2020 CONAE Field Campaign (*C*). For SMAPVEX 2012, the results are divided by crop type: wheat (*a*), corn (*b*), canola (*c*), and soybean (*d*). As for the Yucatan Lake, the findings for both AM (*e*) and PM (*f*) flights are reported.

A. Winnipeg Site: SMAPVEX 2012 Campaign

The results obtained by analyzing the SMAPVEX 2012 dataset depend on the crop type, as also reported in [5], [26], [27], and on the distribution of the fields across the UAVSAR images, which are observed under different incidence angles, even if this effect should be in part mitigated since the polarimetric matrices are calibrated to gamma-naught (i.e., normalized accounting for the local incidence angle). For this reason, as already anticipated in Subsection III-B, the results are reported separately for each crop type. We recall that out of the thirty-one analyzed crop fields, 11 were soybean, 6 wheat, 6 canola, and 8 corn. In the following, the results obtained for each crop type are shown separately.

a) Wheat: The results show that the total descriptors over the wheat fields are characterized by a moderate sensitivity to soil moisture, whereas the most correlated polarimetric descriptor is surprisingly the volume power, independently from the considered decomposition. Regarding the biomass, the volume power is still the most correlated descriptor, while the surface and

TABLE V
Pearson (r) and Spearman's (ρ) Correlation Coefficients Between the Extracted Descriptors and Both Soil Moisture and Wet Biomass for Wheat Fields

Descriptors	SM		Biomass		Descriptors	SM		Biomass	
	r	ρ	r	ρ		r	ρ	r	ρ
α	-0.25	-0.25	**0.34**	**0.32**	P_s^{Y4R}	0.28	0.27	**-0.30**	**-0.37**
H	0.06	0.08	**0.34**	**0.35**	P_d^{Y4R}	0.18	0.19	-0.22	-0.22
γ^0_{HH}	**0.68**	**0.68**	-0.11	-0.13	P_v^{Y4R}	**0.74**	**0.76**	0.34	0.36
γ^0_{HV}	**0.62**	**0.64**	0.42	0.44	P_s^{G4U1}	0.27	0.30	**-0.34**	**-0.44**
γ^0_{VV}	**0.67**	**0.65**	-0.30	-0.32	P_d^{G4U1}	0.14	0.14	-0.13	-0.15
$SPAN$	**0.76**	**0.75**	-0.10	-0.10	P_v^{G4U1}	**0.75**	**0.76**	0.33	0.35
HH/VV	-0.32	-0.27	**0.42**	**0.42**	P_s^{G4U2}	0.29	0.29	**-0.34**	**-0.43**
P_s^{FD}	0.27	0.29	**-0.43**	**-0.48**	P_d^{G4U2}	0.14	0.13	-0.12	-0.14
P_d^{FD}	0.16	0.12	**-0.50**	**-0.60**	P_v^{G4U2}	**0.76**	**0.78**	0.32	0.33
P_v^{FD}	**0.61**	**0.62**	0.46	0.48	P_s^{FDG}	0.28	0.33	**-0.37**	**-0.44**
P_s^{NNED}	**0.33**	**0.36**	**-0.31**	**-0.38**	P_d^{FDG}	0.05	0.03	**-0.20**	**-0.19**
P_d^{NNED}	-0.03	0.01	-0.09	-0.10	P_v^{FDG}	**0.62**	**0.64**	0.42	0.44
P_v^{NNED}	**0.82**	**0.82**	0.17	0.18					

double-bounce terms are characterized by a not negligible negative linear correlation, probably indicating that they are attenuated by the vegetation, even if wheat should be quite transparent to low microwave frequencies [28]. In Table V, the Pearson (r) and Spearman's (ρ) correlation coefficients calculated between all the descriptors and both soil moisture and wet biomass are reported, with the highest correlation values highlighted in gray and bold. It is counterintuitive that, overall, the descriptors with the highest correlation with respect to soil moisture is the volume power P_v both for Pearson (0.61–0.82) and Spearman (0.62–0.82). Regarding the total descriptors, the backscattering coefficients γ^0_{HH} and γ^0_{VV}, and the SPAN are the most correlated to soil moisture (0.68, 0.67, and 0.76); even the backscattering coefficient γ^0_{HV} has a fairly large correlation with soil moisture (0.62), which is higher than the linear correlation of surface and double-bounce powers from the decompositions. The cross polarization has a moderate positive correlation (0.42–0.44) with respect to biomass, as it is driven by volume scattering, whereas the copolarized backscatter has a negative, although very small, correlation, which indicates the predominant effect of the attenuation of the wheat plants.

The H and α descriptors do not exhibit significant correlations (on the order of 0.25–0.35 in absolute value), except for the fact that the alpha angle is characterized by a negative correlation with soil moisture (-0.25). However, it is interesting to note that even if the correlations of H and α are very low, the mean values of both descriptors, considering all the wheat fields and the UAVSAR acquisitions, are 0.82 and 44.43°, respectively: both values indicates predominance of multiple scattering, or volume scattering; considering that the wheat should be quite transparent to low microwave frequencies, this outcome could be related to high values of the surface roughness rather than the vegetation scattering. Indeed, the mean value of the soil roughness standard deviation (σ_z) of the wheat field is 1.15 cm, whilst the correlation

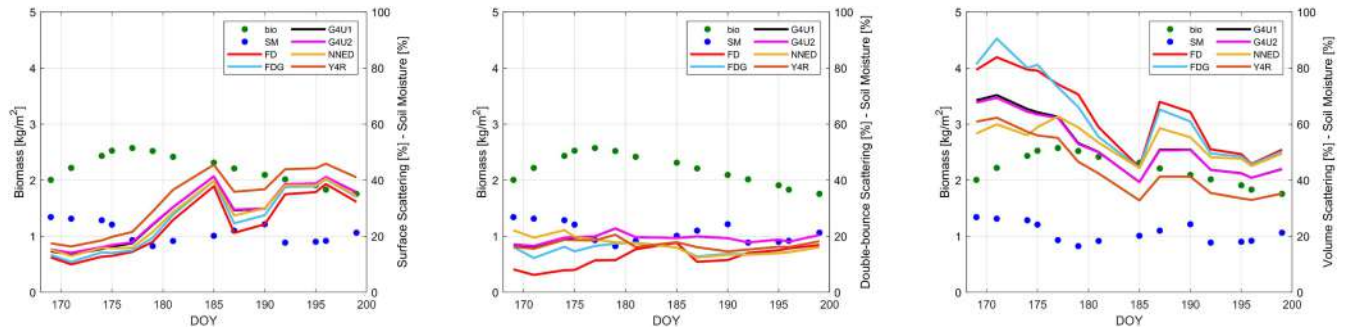

Fig. 5. Temporal evolution of the mean percentage of surface (left), double-bounce (middle), and volume contributions (right) for the six model-based decompositions (Freeman-Durden , FDG, G4U1, G4U2, NNED, Y4R) for wheat fields. Soil moisture and wet biomass are also reported in blue and green, respectively. The x-axis indicates the day of year.

length (l) is 10.96 cm. Regarding the biomass, the volume power has a low to moderate correlation, comparable to that of γ^0_{HV} for some of the decomposition, which is in accordance with the fact that the wheat plants are, again, quite transparent at L-band and characterized by small elements producing a negligible scattering but able to attenuate the signal as the vegetation grows. This attenuation could be the reason for the negative correlation between both the surface and double-bounce terms and the biomass. Fig. 5 reports the temporal trend (i.e., average over different fields) of the mean percentage of surface, double-bounce, and volume powers, calculated with respect to the SPAN, for the six model-based decompositions. The soil moisture (%) and wet biomass (kg/m^2) measurements over time are also reported. To ease the interpretation and highlight the full temporal trend, a linear interpolation is performed to fill the dates where soil moisture and biomass were not collected. Although the wheat is known to be mostly transparent at L band, the predominance of volume scattering is apparent, as also reported in [5], [27], whereas the double-bounce has a fairly low value and constant trend. It is noticeable, however, that in Fig. 5 the spatial mean of the temporal trend of the surface is increasing over time, especially starting from day of year (DOY) 179: this is probably due to the decrease of the wheat wet biomass during the senescent period that attenuates less the surface scattering. To verify whether the combination of polarimetric descriptors is effective in distinguishing changes in soil moisture from those of vegetation, the two linear regression models described by (2) and (3) were applied to retrieve soil moisture for the wheat fields. In (3), the three contributions from the G4U2 were used since it was the decomposition with overall higher linear correlation with SM. Fig. 6 shows the results of this exercise for the case in which the three decomposition powers (dB) and the three gamma-naught terms (dB) were used. Table VI summarizes the results by considering all the decomposition powers and gamma-naught combinations: the Pearson linear correlation (r), the p-value, and the RMSE values between estimated and measured soil moisture are reported.

The best result is obtained when the three G4U2 decomposition powers (P_s^{G4U2}, P_d^{G4U2}, P_v^{G4U2}) are considered for the linear regression ($r = 0.87, p < 0.01, \mathrm{RMSE} = 3.68\%$), again highlighting the importance of the volume term in terms

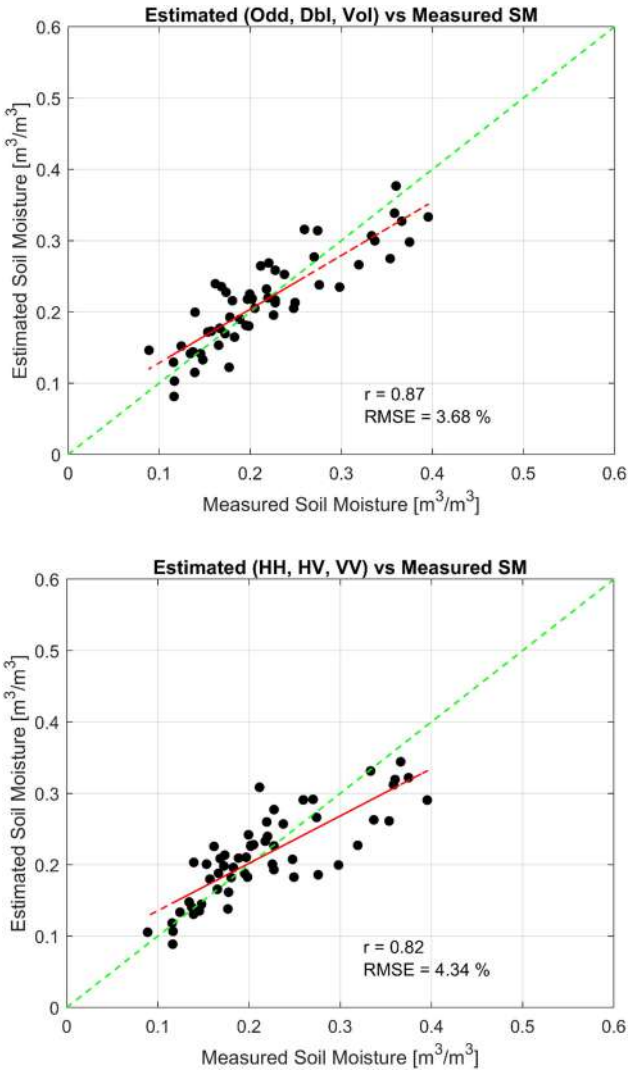

Fig. 6. Results of the two linear regression models applied to wheat fields (estimated versus measured SM). The red line represents the best fit, while the green line is the best agreement between the data. Top: results obtained by considering the surface (Odd), double-bounce (Dbl), and volume (Vol) powers (dB) from the G4U2. Bottom: results obtained by considering the gamma-naught at HH, HV, VV polarizations (dB). The Pearson linear correlation (r), and the RMSE are also displayed.

TABLE VI
RESULTS OF A LINEAR REGRESSION MODEL FOR ESTIMATING THE SOIL MOISTURE FOR THE WHEAT FIELDS BY CONSIDERING A COMBINATIONS OF THE G4U2 DECOMPOSITION POWERS AND A COMBINATIONS OF THE MEASURED BACKSCATTERING COEFFICIENTS

Input	r	p	$RMSE$ (%)
P_s^{G4U2}	0.29	3.2249e-02	7.24
P_d^{G4U2}	0.14	3.1228e-01	7.49
P_s^{G4U2}, P_d^{G4U2}	0.29	3.1334e-02	7.24
P_s^{G4U2}, P_d^{G4U2}, P_v^{G4U2}	**0.87**	**1.6821e-18**	**3.68**
γ^0_{HH}	0.68	1.1136e-08	5.56
γ^0_{HV}	0.62	4.3828e-07	5.96
γ^0_{VV}	0.67	2.0895e-08	5.63
γ^0_{HH}, γ^0_{HV}	0.77	2.5471e-12	4.78
γ^0_{HH}, γ^0_{VV}	0.70	2.4939e-09	5.42
γ^0_{HV}, γ^0_{VV}	**0.82**	**1.1349e-14**	**4.34**
γ^0_{HH}, γ^0_{HV}, γ^0_{VV}	0.82	1.1801e-14	4.34

TABLE VII
PEARSON (r) AND SPEARMAN'S (ρ) CORRELATION COEFFICIENTS BETWEEN THE EXTRACTED DESCRIPTORS AND BOTH SOIL MOISTURE AND WET BIOMASS FOR CORN FIELDS

Descriptors	SM		Biomass		Descriptors	SM		Biomass	
	r	ρ	r	ρ		r	ρ	r	ρ
α	-0.02	0.01	**0.48**	0.33	P_s^{Y4R}	**0.37**	0.33	**0.51**	**0.49**
H	**-0.49**	**-0.50**	**0.65**	**0.72**	P_d^{Y4R}	0.28	0.27	**0.59**	**0.50**
γ^0_{HH}	0.08	0.07	**0.80**	**0.79**	P_v^{Y4R}	-0.11	-0.10	**0.81**	**0.85**
γ^0_{HV}	-0.03	-0.01	**0.78**	**0.77**	P_s^{G4U1}	**0.42**	**0.38**	**0.40**	**0.39**
γ^0_{VV}	**0.42**	**0.41**	**0.50**	**0.43**	P_d^{G4U1}	0.26	0.25	**0.61**	**0.52**
$SPAN$	0.21	0.19	**0.73**	**0.68**	P_v^{G4U1}	-0.07	-0.06	**0.82**	**0.84**
HH/VV	-0.28	-0.30	**0.70**	**0.77**	P_s^{G4U2}	**0.38**	0.34	**0.49**	**0.47**
P_s^{FD}	**0.40**	**0.37**	0.24	0.29	P_d^{G4U2}	0.26	0.25	**0.61**	**0.51**
P_d^{FD}	0.30	0.26	**0.58**	**0.50**	P_v^{G4U2}	-0.08	-0.08	**0.82**	**0.84**
P_v^{FD}	-0.04	-0.02	**0.77**	**0.77**	P_s^{FDG}	**0.39**	**0.37**	0.22	0.27
P_s^{NNED}	**0.38**	**0.37**	0.26	0.29	P_d^{FDG}	0.27	0.24	**0.59**	**0.50**
P_d^{NNED}	0.26	0.23	**0.59**	**0.50**	P_v^{FDG}	-0.03	-0.01	**0.78**	**0.77**
P_v^{NNED}	-0.01	0	**0.79**	**0.78**					

of sensitivity to soil moisture. For the total descriptors, the best result is obtained when the two gamma-naught terms γ^0_{HV} and γ^0_{VV} are exploited ($r = 0.82$, $p < 0.01$, RMSE $= 4.34\%$); when γ^0_{HH} is added in the exercise, the result remains the same, as expected considering that the double-bounce mechanism is negligible (see Fig. 5) and, for this reason, it does not carry information on biomass as compared to γ^0_{VV} (see Table V).

b) Corn: The results show that all the extracted descriptors, both total and polarimetric, exhibit a large linear correlation with the wet biomass. The correlation values are large even when the Spearman's correlation is considered, thus indicating that the relationship could be not purely linear. The sensitivity to soil moisture is different with respect to wheat, with the surface power being the most correlated polarimetric parameter as one could expect. Table VII reports the Pearson (r) and Spearman (ρ) correlation coefficients between each of the descriptors and both soil moisture and wet biomass, with the highest correlation values highlighted in gray and bold. If the correlation with the soil moisture is analyzed, the corn backscattering coefficient γ^0_{VV} is overall the descriptor that shows the higher positive linear correlation; the γ^0_{HV}, and surprisingly the coefficient γ^0_{HH}, exhibit no correlation. This may be explained by the fact that γ^0_{HH} and γ^0_{HV} are more influenced by vegetation, as also confirmed by the correlation values reported in Table VII for those descriptors. Among the polarimetric descriptors, the surface power is the most correlated to soil moisture variations, even if the values are small ($r = 0.37$ - 0.42). Even the double-bounce power shows low values of correlation with soil moisture ($r = 0.26$ - 0.30), while the volume contributions, as expected and differently from the wheat fields, show no correlation with moisture.

For both double-bounce and volume terms, these results indicate that they are more influenced by the canopy and the vertical structure of the corn plant, as confirmed by the high linear correlation with the wet biomass (0.58–0.61 for double-bounce, 0.77–0.82 for volume). The total backscattering coefficients γ^0_{HH} and γ^0_{HV} are characterized by a large linear correlation with the measured biomass (0.80 and 0.78, respectively), while γ^0_{VV} shows smaller correlation values, similar to the ones with soil moisture. The high correlation of γ^0_{HH} with vegetation parameters, hiding its sensitivity to moisture, is likely due to the increasing interaction between the ground and the vertical and large stems, which for corn seem to retain more the effect of vegetation growth rather than that of change in soil reflection. Regarding the polarimetric decompositions, it remains challenging to justify the appreciable positive correlation (0.22–0.51) between the surface contribution and the biomass; this was not observed for the wheat fields, where on the contrary a moderate negative correlation was justified by the attenuation of the surface scattering. A high correlation with the wet biomass is also observed for the alpha angle (0.48), and especially for entropy; in this case, the Spearman's correlation is slightly higher with respect to the Pearson's value, again highlighting that the relationship between entropy and biomass is not purely linear. Fig. 7 reports the temporal trend (i.e., average over different fields) of the mean percentage of surface, double-bounce, and volume powers, calculated with respect to the SPAN, for the six model-based decompositions. The soil moisture (%) and biomass (kg/m^2) measurements over time are also reported, linearly interpolated to fill the dates where the two variables were not collected. It can be noted that there are some differences between the behavior of the different decompositions involved in the analysis. For Freeman-Durden , FDG, and NNED the volume scattering seems dominant for almost the entire period; indeed, from the literature, Freeman-Durden is known to overestimate the volume contribution. For the other decompositions (G4U1, G4U2, and Y4R), when the biomass values remain below approximately 1 kg/m^2, volume scattering is at a minimum, as expected, whereas surface and double-bounce terms are dominant. The high double-bounce cannot be justified in the first days when the plants are in an early stage, but then it starts decreasing more rapidly than the surface power from about DOY 175. Then, the double-bounce starts to increase again, this time in accordance with the increasing interaction between the ground and the grown vertical structure of the corn plants.

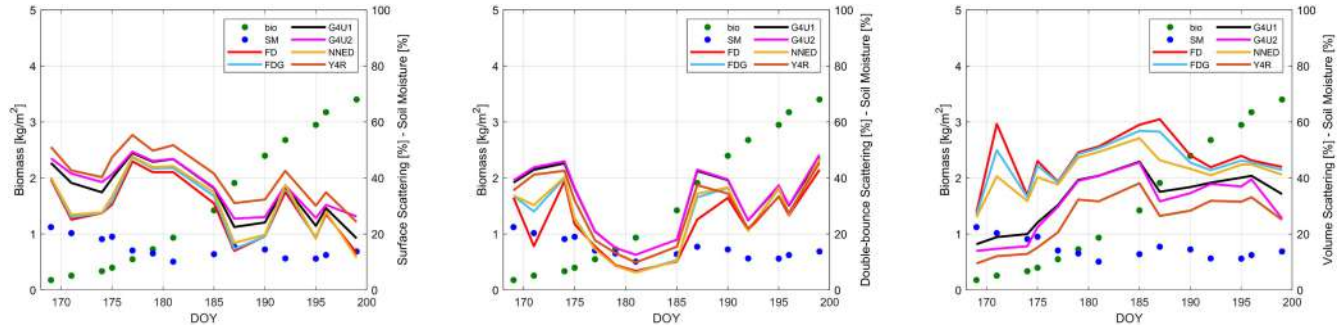

Fig. 7. Temporal evolution of the mean percentage of surface (left), double-bounce (middle), and volume contributions (right) for the six model-based decompositions (FD, FDG, G4U1, G4U2, NNED, Y4R) for corn fields. Soil moisture and wet biomass are also reported in blue and green, respectively. The *x*-axis indicates the day of year.

TABLE VIII
RESULTS OF A LINEAR REGRESSION MODEL FOR ESTIMATING THE SOIL MOISTURE FOR THE CORN FIELDS BY CONSIDERING A COMBINATIONS OF THE G4U1 DECOMPOSITION POWERS AND A COMBINATIONS OF THE MEASURED BACKSCATTERING COEFFICIENTS

Input	r	p	$RMSE$ (%)
P_s^{G4U1}	0.42	8.7613e-05	5.23
P_d^{G4U1}	0.26	1.7503e-02	5.55
P_s^{G4U1}, P_d^{G4U1}	0.42	6.4672e-05	5.21
P_s^{G4U1}, P_d^{G4U1}, P_v^{G4U1}	**0.67**	**5.6328e-12**	**4.28**
γ_{HH}^0	0.08	4.7194e-01	5.73
γ_{HV}^0	0.03	7.9974e-01	5.75
γ_{VV}^0	0.42	7.7759e-05	5.21
γ_{HH}^0, γ_{HV}^0	0.27	1.5248e-02	5.54
γ_{HH}^0, γ_{VV}^0	0.54	1.2356e-07	4.83
γ_{HV}^0, γ_{VV}^0	**0.65**	**2.1784e-11**	**4.35**
γ_{HH}^0, γ_{HV}^0, γ_{VV}^0	**0.66**	**8.5663e-12**	**4.31**

As for the volume scattering, especially for G4U1, G4U2, and Y4R, it closely follows the biomass trend until approximately DOY 185, as also expressed by the high correlation values in Table VII, and then it reaches a level of saturation, contrarily to double-bounce scattering. It is noteworthy the behavior of the surface term, which is decreasing for increasing biomass (although only after DOY 175), but it also shows a behavior opposite to the double-bounce in the interval from DOY 185 to 190. It is apparent a sort of "cross-talk" between the surface and double-bounce components in the considered decompositions. The two linear regression models described by (2) and (3) were then applied to assess whether the combination of total or polarimetric descriptors best highlight soil moisture changes in corn fields. As for the decomposition powers, the G4U1 was used since it was the decomposition with the highest linear correlation with respect to the measured soil moisture for the surface term. Fig. 8 shows the results of this exercise for the case in which the three decomposition powers (dB) and the three gamma-naught terms (dB) were used. Table VIII summarizes the results by considering all the decomposition powers and gamma-naught combinations: the Pearson linear correlation (r), the p-value, and the RMSE values between estimated and measured soil moisture are reported.

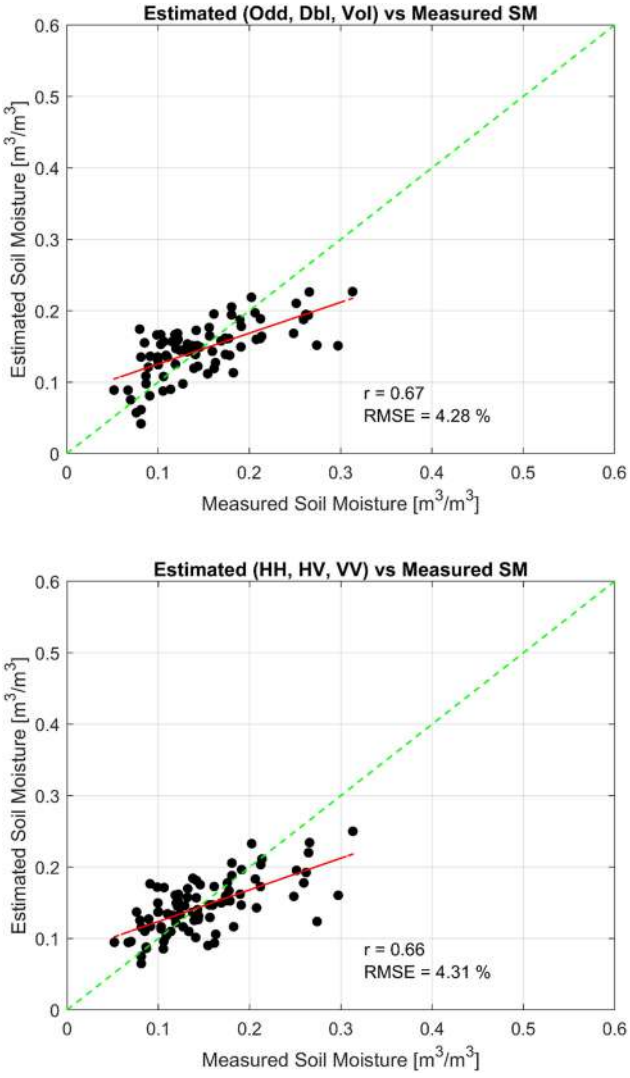

Fig. 8. Results of the two linear regression models applied to corn fields (estimated versus measured SM). The red line represents the best fit, while the green line is the best agreement between the data. Top: results obtained by considering the surface (Odd), double-bounce (Dbl), and volume (Vol) powers (dB) from the G4U1. Bottom: results obtained by considering the gamma-naught at HH, HV, VV polarizations (dB). The Pearson linear correlation (r), and the RMSE are also displayed.

TABLE IX
PEARSON (r) AND SPEARMAN'S (ρ) CORRELATION COEFFICIENTS BETWEEN THE EXTRACTED DESCRIPTORS AND BOTH SOIL MOISTURE AND WET BIOMASS FOR CANOLA FIELDS

Descriptors	SM		Biomass		Descriptors	SM		Biomass	
	r	ρ	r	ρ		r	ρ	r	ρ
α	0.11	0.08	**0.37**	**0.33**	P_s^{Y4R}	-0.20	-0.07	**-0.50**	**-0.44**
H	0.20	0.17	0.13	0.15	P_d^{Y4R}	0.06	0.04	0.06	-0.07
γ^0_{HH}	0.13	0.16	0.15	0.03	P_v^{Y4R}	0.19	0.17	**0.28**	**0.27**
γ^0_{HV}	0.19	0.17	**0.27**	**0.24**	P_s^{G4U1}	-0.21	-0.06	**-0.51**	**-0.46**
γ^0_{VV}	**0.27**	**0.27**	-0.07	-0.12	P_d^{G4U1}	0.01	-0.01	0.06	-0.07
$SPAN$	0.20	0.21	0.12	0.05	P_v^{G4U1}	0.20	0.18	**0.27**	**0.25**
HH/VV	-0.27	-0.23	0.33	0.25	P_s^{G4U2}	-0.20	-0.06	**-0.51**	**-0.46**
P_s^{FD}	-0.10	-0.04	**-0.77**	**-0.65**	P_d^{G4U2}	0.01	-0.01	0.06	-0.07
P_d^{FD}	0.06	0.05	**-0.61**	**-0.57**	P_v^{G4U2}	0.19	0.18	**0.27**	**0.25**
P_v^{FD}	0.14	0.14	**0.34**	**0.30**	P_s^{FDG}	-0.18	-0.04	**-0.52**	**-0.41**
P_s^{NNED}	-0.19	-0.09	**-0.36**	**-0.24**	P_d^{FDG}	0.01	-0.01	0.19	0.08
P_d^{NNED}	0.05	0.07	0.12	0.05	P_v^{FDG}	0.19	0.17	**0.27**	**0.24**
P_v^{NNED}	0.23	0.22	0.07	0.09					

The best result is obtained when the three decomposition powers (P_s^{G4U1}, P_d^{G4U1}, P_v^{G4U1}) are considered ($r = 0.67$, $p < 0.01$, RMSE $= 4.28\%$), although a very similar result is also obtained when the three gamma-naught terms (γ^0_{HH}, γ^0_{HV}, γ^0_{VV}) are considered ($r = 0.66$, $p < 0.01$, RMSE $= 4.31\%$). In the latter case, the estimates do not change significantly after removing γ^0_{HH} and using the pair (γ^0_{HV}, γ^0_{VV}), underlying again the predominant influence of vegetation growth on γ^0_{HH}. When considering the decomposition powers, one can observe that in corn fields the soil moisture retrieval performances are driven by the surface mechanism, while the double-bounce term confirms not being able to give any direct contribution, as it is mainly driven by the plant growth. Instead, double-bounce itself (as well as γ^0_{HH}) and, especially, the volume scattering mechanisms help disentangling the effect of the vegetation from that of soil moisture.

c) Canola: Retrieving biogeophysical parameters of this crop revealed to be very challenging. The results show that the Pearson and Spearman correlations between any extracted descriptor and both soil moisture and biomass are generally low, except in some cases in which a large negative correlation is obtained. Table IX reports the Pearson (r) and Spearman's (ρ) correlation coefficients between the descriptors and both soil moisture and wet biomass, with the highest correlation values highlighted in gray and bold. The correlation of all descriptors with soil moisture is always very small and sometimes even negative. Only γ^0_{VV} exhibits moderate positive correlations. It is interesting to note that the surface powers from the six model-based decompositions are characterized by a negative correlation with respect to biomass, both for Pearson (-0.77, -0.36) and Spearman (-0.65, -0.24) coefficients. Indeed, when the biomass exhibits high values, it is expected the surface scattering be attenuated leading to the negative correlation, as already noted in the wheat fields, although at a much smaller extent. A large negative correlation with the biomass is also observed for the double-bounce retrieved by the Freeman-Durden decomposition.

The other polarimetric descriptors exhibit not as much significant correlation with biomass, except for the volume term and the alpha angle, even if the correlation values are not so high. Fig. 9 reports the temporal trend (i.e., average over different fields) of the mean percentage of surface, double-bounce, and volume powers, calculated with respect to the SPAN, for the six model-based decompositions. The soil moisture (%) and biomass (kg/m^2) measurements over time are also reported, linearly interpolated to fill the dates where the two variables were not collected. It is possible to note that the volume term is dominant in all UAVSAR acquisitions, even during the first days with smaller biomass, but then decreases in agreement with the biomass. The double-bounce power is much lower than the volume power and it also shows a very low correlation with biomass: this could be explained by the fact that canola is characterized by rounded leaves and a complex plant structure that does not support the onset of the dihedral scattering mechanism. Until approximately DOY 185, the double-bounce from Freeman-Durden is characterized by a different trend with respect to the other decompositions, which explains the unique large negative correlation with respect to the biomass. Some other interesting observations could be made. During the first acquisitions the biomass increases over time but the surface contribution remains low; as the biomass decreases, the surface scattering progressively increases over time, which was explained in [5], [27] by the fact that the canola fields undergo a drying out process that makes the soil being less attenuated; nonetheless, the fact that the surface power does not return to the level of the first quite moist days indicates that the contribution of the volume is likely contaminating the results of the decompositions. It is also interesting to note that the double-bounce term seems to slightly decrease and therefore to capture this plant drying phenomena (see Fig. 9, middle) that diminishes the interaction with the stems involved in one of the two bounces. However, the quite opposite behavior in the interval from DOY 180 to 185 of surface and double-bounce components could be again the effect of "scattering mechanisms cross-talk", a shortcoming of the decomposition algorithms that do not correctly disentangle the two mechanisms. The two linear regression models described by (2) and (3) were again applied to retrieve soil moisture by considering alternatively as predictors a combination of the backscattering coefficients gamma-naught at HH, HV, VV polarizations or a combination of the polarimetric surface (Odd), double-bounce (Dbl), and volume (Vol) powers obtained after applying the G4U1. The latter was the decomposition with higher linear correlation of both surface and volume contributions with respect to the measured soil moisture. Fig. 10 shows the results of this exercise for the case in which the three decomposition powers (dB) and the three gamma-naught terms (dB) were used. Table X summarizes the results by considering all the decomposition powers and gamma-naught combinations: the Pearson linear correlation (r), the p-value, and the RMSE values between estimated and measured soil moisture are reported.

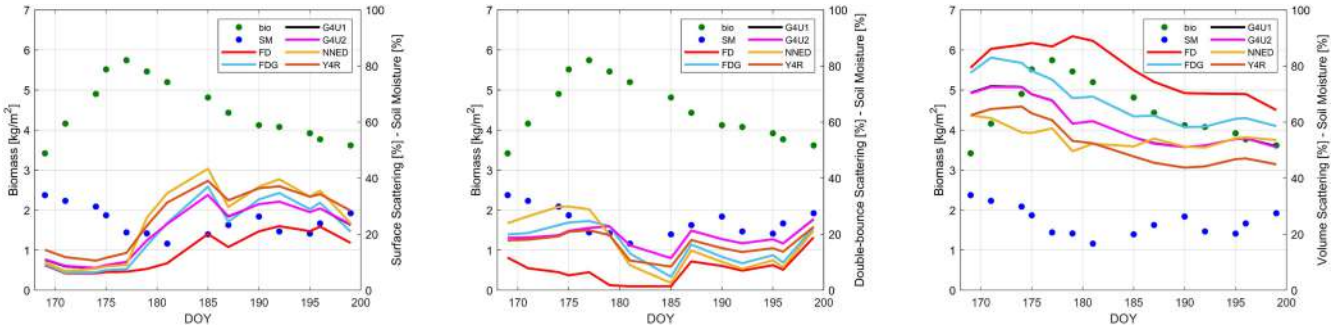

Fig. 9. Temporal evolution of the mean percentage of surface (left), double-bounce (middle), and volume contributions (right) for the six model-based decompositions (FD, FDG, G4U1, G4U2, NNED, Y4R) for canola fields. Soil moisture and wet biomass are also reported in blue and green, respectively. The *x*-axis indicates the day of year.

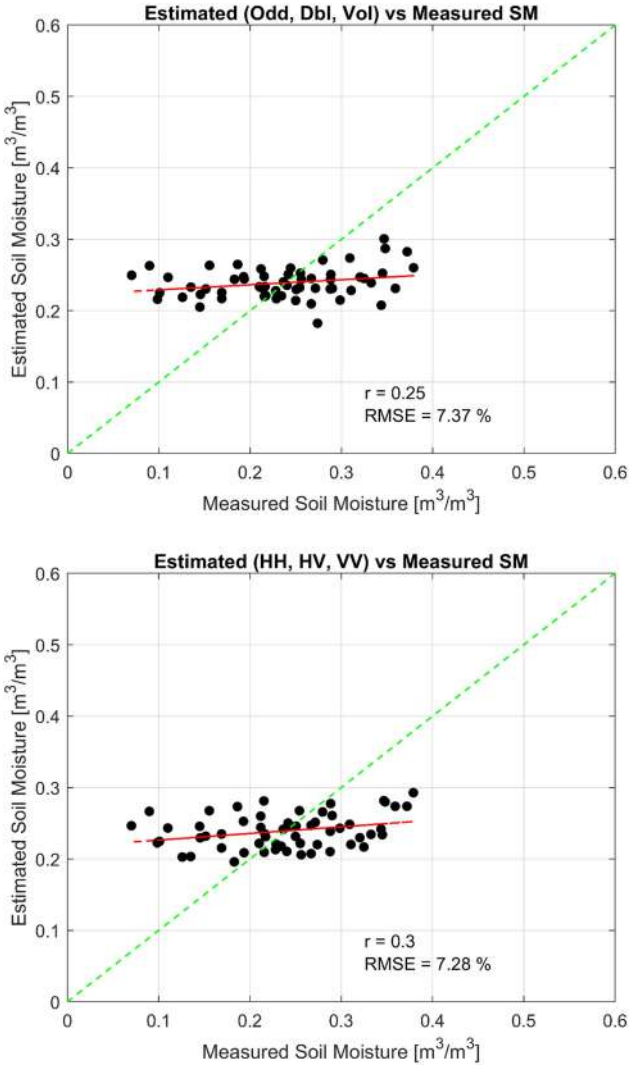

Fig. 10. Results of the two linear regression models applied to canola fields (estimated versus measured SM). The red line represents the best fit, while the green line is the best agreement between the data. Top: results obtained by considering the surface (Odd), double-bounce (Dbl), and volume (Vol) powers (dB) from the G4U1. Bottom: results obtained by considering the gamma-naught at HH, HV, VV polarizations (dB). The Pearson linear correlation (r), and the RMSE are also displayed.

TABLE X
RESULTS OF A LINEAR REGRESSION MODEL FOR ESTIMATING THE SOIL MOISTURE FOR THE CANOLA FIELDS BY CONSIDERING A COMBINATIONS OF THE G4U1 DECOMPOSITION POWERS AND A COMBINATIONS OF THE MEASURED BACKSCATTERING COEFFICIENT

Input	r	p	$RMSE$ (%)
P_s^{G4U1}	0.21	1.1719e-01	7.45
P_d^{G4U1}	0.01	9.4644e-01	7.62
P_s^{G4U1}, P_d^{G4U1}	0.22	1.0246e-01	7.44
P_s^{G4U1}, P_d^{G4U1}, P_v^{G4U1}	**0.25**	**5.3829e-02**	**7.37**
γ^0_{HH}	0.13	3.2008e-01	7.55
γ^0_{HV}	0.19	1.4738e-01	7.48
γ^0_{VV}	0.27	4.4362e-02	7.35
γ^0_{HH}, γ^0_{HV}	0.20	1.2590e-01	7.46
γ^0_{HH}, γ^0_{VV}	**0.30**	**2.3317e-02**	**7.28**
γ^0_{HV}, γ^0_{VV}	0.27	3.7181e-02	7.33
γ^0_{HH}, γ^0_{HV}, γ^0_{VV}	**0.30**	**2.3342e-02**	**7.28**

The best result is obtained when the three gamma-naught terms (γ^0_{HH}, γ^0_{HV}, γ^0_{VV}) are involved ($r = 0.30$, $p \cong 0.02$, $\mathrm{RMSE} = 7.28\%$); it is interesting to note that the same result is achieved if γ^0_{HV} is removed from the model, showing that as for canola the cross-polarization does not bring independent information in terms of sensitivity to soil moisture, since it is likely more influenced by the vegetation, as shown in Table IX. Overall, the retrieval is characterized by a poor statistic, as also confirmed by the low inversion rate obtained in [27] for retrieving soil moisture for canola fields.

d) Soybean: Soybean is also a very challenging crop for what concerns soil moisture retrieval. The correlation coefficients given by both Pearson (r) and Spearman (ρ) are computed and their values are reported in Table XI. The highest correlation values are highlighted in gray and bold.

It is immediately apparent the very low correlation of all the descriptors with soil moisture. Some correlation, although negative, is surprisingly observed for all the volume power terms of the decompositions, the two backscattering coefficients γ^0_{HH} and γ^0_{HV}, the entropy and the alpha angle. The correlation between the volume contribution or the γ^0_{HV} and soil moisture

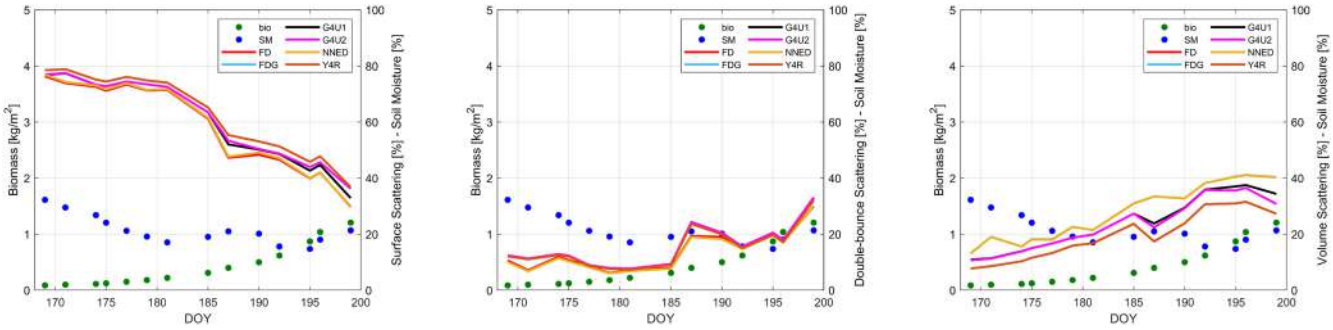

Fig. 11. Temporal evolution of the mean percentage of surface (left), double-bounce (middle), and volume contributions (right) for the six model-based decompositions (FD, FDG, G4U1, G4U2, NNED, Y4R) for soybean fields. Soil moisture and wet biomass are also reported in blue and green, respectively. The x-axis indicates the day of year.

TABLE XI
PEARSON (r) AND SPEARMAN'S (ρ) CORRELATION COEFFICIENTS BETWEEN THE EXTRACTED DESCRIPTORS AND BOTH SOIL MOISTURE AND WET BIOMASS FOR SOYBEAN FIELDS

Descriptors	SM		Biomass		Descriptors	SM		Biomass	
	r	ρ	r	ρ		r	ρ	r	ρ
α	-0.14	-0.12	**0.71**	**0.73**	P_s^{Y4R}	-0.02	-0.06	0.05	0.07
H	-0.26	-0.20	**0.59**	**0.77**	P_d^{Y4R}	-0.10	-0.07	**0.71**	**0.67**
γ_{HH}^0	-0.27	-0.26	**0.57**	**0.60**	P_v^{Y4R}	-0.34	-0.34	**0.69**	**0.81**
γ_{HV}^0	-0.31	-0.29	**0.70**	**0.79**	P_s^{G4U1}	-0.01	-0.06	0	0.03
γ_{VV}^0	0.01	-0.01	**0.34**	**0.26**	P_d^{G4U1}	-0.10	-0.08	**0.72**	**0.68**
$SPAN$	-0.12	-0.12	**0.47**	**0.43**	P_v^{G4U1}	-0.33	-0.32	**0.70**	**0.80**
HH/VV	**-0.45**	**-0.46**	0.28	0.51	P_s^{G4U2}	-0.01	-0.05	0.07	0.06
P_s^{FD}	0.01	-0.04	-0.07	-0.05	P_d^{G4U2}	-0.10	-0.08	**0.72**	**0.68**
P_d^{FD}	-0.15	-0.13	**0.73**	**0.72**	P_v^{G4U2}	-0.34	-0.32	**0.65**	**0.79**
P_v^{FD}	-0.31	-0.29	**0.70**	**0.79**	P_s^{FDG}	0.01	-0.04	-0.09	-0.06
P_s^{NNED}	0.01	-0.04	-0.09	-0.06	P_d^{FDG}	-0.15	-0.13	**0.74**	**0.73**
P_d^{NNED}	-0.15	-0.13	**0.74**	**0.73**	P_v^{FDG}	-0.31	-0.29	**0.70**	**0.79**
P_v^{NNED}	-0.32	-0.30	**0.70**	**0.79**					

could be ascribed to a correlation between water in the soil and water retained by the vegetation or captured from precipitation or irrigation events that increases absorption. Note that a very small negative correlation of the volume term with soil moisture was also observed for corn fields in Table VII, while a large positive correlation of the volume contribution was observed for wheat, as reported in Table V. Conversely, the correlation with wet biomass is overall high and it is interesting that the double-bounce and volume contributions have quite similar correlation values. This is not completely unexpected also considering the contribution of the pods to the double-bounce, as discussed in [29]. Instead, the surface power appears to be uncorrelated with vegetation: while this may be expected, it is worth noting that the increasing attenuation with biomass is not producing any negative correlation as observed in other crops. Moreover, although the surface contribution is the one showing the highest power, as reported in Fig. 11, it is not correlated with soil moisture. It is interesting to note that the copolarization ratio of HH to VV exhibits a non-negligible negative correlation with soil moisture (-0.45). Finally, the correlation of the alpha angle and entropy with respect to the wet biomass is high, as expected; in this case, the larger values obtained when the Spearman's correlation is involved, especially for the entropy, likely highlights a nonlinear relationship with the vegetation. Fig. 11 reports the temporal trend (i.e., average over different fields) of the mean percentage of surface, double-bounce, and volume powers, calculated with respect to the SPAN, for the six model-based decompositions. The soil moisture (%) and biomass (kg/m^2) measurements over time are also reported, linearly interpolated to fill the dates where soil moisture and biomass were not collected. The surface scattering decreases over time probably due to the attenuation introduced by the increasing wet biomass, even if it reaches a maximum value of approximately 1 kg/m^2. The double-bounce and volume contributions follow the biomass trend over time, even if the latter seems to reach a level of saturation, as also observed for corn fields. It is noticeable, however, that in Fig. 11 the temporal trend of the surface is almost correlated to soil moisture even if Table XI shows no correlation of the surface terms with moisture. The two linear regression models described by (2) and (3) were applied to retrieve soil moisture by considering alternatively as predictors a combination of the backscattering coefficients gamma-naught or the polarimetric surface (Odd), double-bounce, and volume powers obtained by applying the NNED. This decomposition was the one with the highest linear correlation of surface and double-bounce contributions with respect to soil moisture. Fig. 12 shows the results of this exercise for the case in which the three decomposition powers (dB) and the three gamma-naught terms (dB) were used. Table XII summarizes the results by considering all the decomposition powers and gamma-naught combinations: the Pearson linear correlation (r), the p-value, and the RMSE values between estimated and measured soil moisture are reported. The best result is obtained when the three backscattering coefficients gamma-naught (γ^0_{HH}, γ^0_{HV}, γ^0_{VV}) are involved ($r = 0.50, p < 0.01, \mathrm{RMSE} = 7.59\%$), even if when γ^0_{HV} is removed from the model, a similar result is obtained. When the three decomposition powers (P_s^{NNED}, P_d^{NNED}, P_v^{NNED}) are considered, the results slightly worsen ($r = 0.40, p < 0.01, \mathrm{RMSE} = 8.03\%$) both in terms of linear correlation and RMSE.

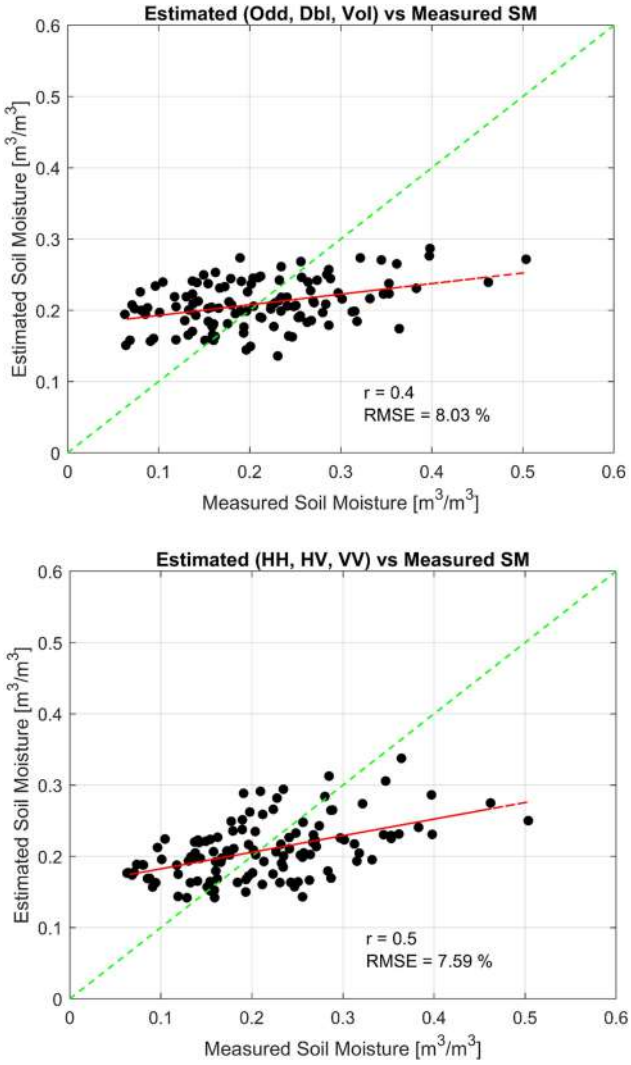

Fig. 12. Results of the two linear regression models applied to soybean fields (estimated versus measured SM). The red line represents the best fit, while the green line is the best agreement between the data. Top: results obtained by considering the surface (Odd), double-bounce (Dbl), and volume (Vol) powers (dB) from the NNED. Bottom: results obtained by considering the gamma-naught at HH, HV, VV polarizations (dB). The Pearson linear correlation (r), and the RMSE are also displayed.

B. Yucatan Lake Site: 2019 NISAR AM/PM Campaign

Ground truth data were not available over this site so that the correlation analysis was done considering the Soil Water Index from the C-band ASCAT sensor onboard the Metop satellites, and the NDVI from Sentinel-2 linearly interpolated at the time of the UAVSAR overpasses. We recall that the SWI is characterized by a coarse resolution (12.5 km) and distinction between crop types was not possible, so that the results describe an overall behavior of an agricultural vegetated area. The analysis is carried out by separating AM and PM flights since they are characterized by different flight directions and, consequently, different values of the incidence angle (about 53° in average for the AM flights, about 25° in average for the PM flights). Since the sigma-naught strongly depends on the incidence angle, the gamma-naught normalization allows to neglect the difference in incidence angle in our comparison among different feature selections, including the difference between the AM and PM flights.

TABLE XII
RESULTS OF A LINEAR REGRESSION MODEL FOR ESTIMATING THE SOIL MOISTURE FOR THE SOYBEAN FIELDS BY CONSIDERING A COMBINATIONS OF THE NNED DECOMPOSITION POWERS AND A COMBINATIONS OF THE MEASURED BACKSCATTERING COEFFICIENTS

Input	r	p	$RMSE$ (%)
P_s^{NNED}	0.01	8.9029e-01	8.76
P_d^{NNED}	0.15	1.0620e-01	8.66
P_s^{NNED}, P_d^{NNED}	0.15	1.0587e-01	8.66
$\boldsymbol{P_s^{NNED}, P_d^{NNED}, P_v^{NNED}}$	**0.40**	**9.2669e-06**	**8.03**
γ_{HH}^0	0.27	2.7006e-03	8.41
γ_{HV}^0	0.31	5.6732e-04	8.31
γ_{VV}^0	0.01	9.3061e-01	8.76
$\gamma_{HH}^0, \gamma_{HV}^0$	0.31	5.9760e-04	8.31
$\boldsymbol{\gamma_{HH}^0, \gamma_{VV}^0}$	**0.50**	**9.0937e-09**	**7.58**
$\gamma_{HV}^0, \gamma_{VV}^0$	0.40	7.6669e-06	8.02
$\boldsymbol{\gamma_{HH}^0, \gamma_{HV}^0, \gamma_{VV}^0}$	**0.50**	**9.9582e-09**	**7.59**

e) AM Flights: Table XIII reports the Pearson (r) and Spearman's (ρ) correlation coefficients calculated between both total and polarimetric descriptors and both SWI and interpolated NDVI for the AM flights. The highest correlation values are highlighted in gray and bold. It is possible to note that in this case the polarimetric descriptors exhibit generally better correlation as compared to the total ones. The double-bounce extracted from the six model-based decompositions (FD, NNED, Y4R, G4U1, G4U2, FDG) shows the highest linear correlation with the SWI variations (0.80–0.82) because of the changing permittivity and reflection from the soil. The volume power exhibits the highest linear correlation with the interpolated NDVI (0.77–0.80), although the correlation value is very similar to that of the γ_{HV}^0 (0.78): this is an expected result since signal depolarization mostly drives the retrieval of the vegetation volume scattering contribution with respect to the copolarized returns. It is noticeable that also the double-bounce has a large linear correlation with the NDVI (0.73–0.74), due to the interaction with the vertical structure of the vegetation, as already observed, e.g., for the corn and soybean fields in SMAPVEX 2012 data. The combined effect of both the soil reflection and the vegetation interaction contributing to the dihedral effect is apparent in this dataset where the crop type is, however, not distinguished.

It is interesting to note that also the volume power is characterized by a large correlation with the SWI (0.65–0.71). This result was also observed previously for the wheat fields of SMAPVEX 2012 (see Table V), and it could be due to the plant water uptake from the soil or rainwater interception, with a direct influence on the backscattering coefficient at HV polarization, from which the volume contribution is basically derived. It is unexpected that the surface power is not the one having the largest correlation with SWI, as already shown in Table XIII. It exhibits a very low linear correlation (0.18–0.22) with respect to the NDVI, confirming what is expected from the theory; the positive values of the correlation, even if low, could be due to a "cross-talk"

TABLE XIII
PEARSON (r) AND SPEARMAN'S (ρ) CORRELATION COEFFICIENTS BETWEEN THE EXTRACTED DESCRIPTORS AND BOTH SOIL WATER INDEX AND INTERPOLATED NDVI FOR UAVSAR AM FLIGHTS

Descriptors	SWI		Int. NDVI		Descriptors	SWI		Int. NDVI	
	r	ρ	r	ρ		r	ρ	r	ρ
α	**0.67**	**0.69**	0.59	**0.68**	P_s^{Y4R}	**0.40**	0.31	0.22	0.18
H	0.45	0.56	**0.70**	**0.75**	P_d^{Y4R}	**0.82**	0.79	**0.73**	**0.79**
γ^0_{HH}	0.49	0.39	**0.63**	0.52	P_v^{Y4R}	**0.65**	0.59	**0.80**	**0.80**
γ^0_{HV}	0.71	0.65	**0.78**	**0.76**	P_s^{G4U1}	**0.38**	0.26	0.19	0.12
γ^0_{VV}	**0.65**	0.58	0.32	0.34	P_d^{G4U1}	**0.82**	0.79	**0.73**	**0.79**
$SPAN$	**0.63**	0.57	0.50	0.49	P_v^{G4U1}	**0.70**	0.64	**0.78**	**0.76**
HH/VV	**-0.37**	-0.27	0.32	0.20	P_s^{G4U2}	**0.40**	0.31	0.21	0.17
P_s^{FD}	**0.36**	0.23	0.19	0.10	P_d^{G4U2}	**0.82**	0.79	**0.73**	**0.79**
P_d^{FD}	**0.82**	0.78	**0.73**	**0.80**	P_v^{G4U2}	**0.68**	0.59	**0.77**	**0.75**
P_v^{FD}	**0.71**	0.65	**0.78**	**0.76**	P_s^{FDG}	**0.35**	0.24	0.18	0.09
P_s^{NNED}	**0.35**	0.24	0.18	0.09	P_d^{FDG}	**0.80**	0.77	**0.74**	**0.81**
P_d^{NNED}	**0.80**	0.77	**0.74**	**0.81**	P_v^{FDG}	**0.71**	0.65	**0.78**	**0.76**
P_v^{NNED}	**0.71**	0.65	**0.78**	**0.76**					

TABLE XIV
RESULTS OF A LINEAR REGRESSION MODEL FOR ESTIMATING THE SOIL WATER INDEX FOR THE AM FLIGHTS BY CONSIDERING A COMBINATION OF THE FREEMAN-DURDEN DECOMPOSITION POWERS AND A COMBINATION OF THE MEASURED BACKSCATTERING COEFFICIENTS

Input	r	p	$RMSE$ (%)
P_s^{FD}	0.36	1.7995e-02	14.42
P_d^{FD}	0.82	2.5270e-11	8.82
P_s^{FD}, P_d^{FD}	0.82	2.2711e-11	8.79
P_s^{FD}, P_d^{FD}, P_v^{FD}	**0.83**	**1.7877e-11**	**8.74**
γ^0_{HH}	0.49	9.2690e-04	13.49
γ^0_{HV}	0.71	1.5262e-07	10.93
γ^0_{VV}	0.65	3.1872e-06	11.77
γ^0_{HH}, γ^0_{HV}	0.81	1.2207e-10	9.17
γ^0_{HH}, γ^0_{VV}	0.65	3.1767e-06	11.76
γ^0_{HV}, γ^0_{VV}	0.73	4.4589e-08	10.60
γ^0_{HH}, γ^0_{HV}, γ^0_{VV}	**0.86**	**5.4291e-13**	**8.02**

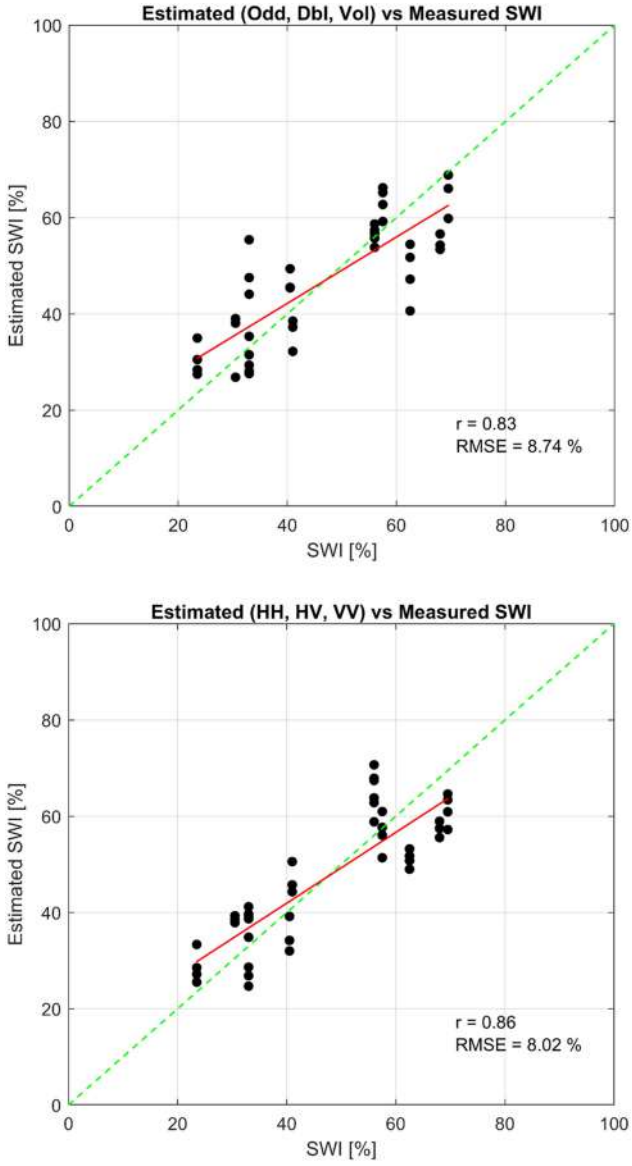

Fig. 13. Results of the two linear regression models applied to the AM flights (estimated versus measured SWI). The red line represents the best fit, while the green line is the best agreement between the data. Top: results obtained by considering the surface (Odd), double-bounce (Dbl), and volume (Vol) powers (dB) from the Freeman-Durden . Bottom: results obtained by considering the gamma-naught at HH, HV, VV polarizations. The Pearson linear correlation (r), and the RMSE are also displayed.

between the surface and volume contributions, so that some of the volume power is assigned to the surface one. The results obtained from the H/α decomposition shows that the entropy has a large correlation with the NDVI (r: 0.70, ρ: 0.75) due to the increase of the target randomness with NDVI, while α has a moderate correlation with SWI (r: 0.67, ρ: 0.68); in addition, the alpha angle exhibits a similar correlation also with respect to the NDVI changes (0.68). The two linear regression models described by (2) and (3) were applied to the AM flights for estimating the SWI. In (3), the three contributions from the FD were used since it was the decomposition with generally the highest linear correlation with SWI. Fig. 13 shows the results of this exercise for the case in which the three decomposition powers (dB) and the three gamma-naught terms (dB) were used. Table XIV summarizes the results by considering all the decomposition powers and gamma-naught combinations: the Pearson linear correlation (r), the p-value, and the RMSE values between estimated and measured SWI are reported.

The estimates obtained considering the three gamma-naught (γ^0_{HH}, γ^0_{HV}, γ^0_{VV}) are slightly better correlated to SWI ($r = 0.86$, $p < 0.01$, RMSE $= 8.02\%$) if compared to the three FD powers (P_s^{FD}, P_d^{FD}, P_v^{FD}) ($r = 0.83$, $p < 0.01$, RMSE $= 8.74\%$). If two powers (P_s^{FD}, P_d^{FD}) are used to estimate SWI, the obtained results are better than the case in which a combination of gamma-naught at two polarizations (γ^0_{HV}, γ^0_{VV} and γ^0_{HH}, γ^0_{VV}) are involved; when using (γ^0_{HH}, γ^0_{HV}) the correlation value and the RMSE are comparable. Combining the three gamma-naught

TABLE XV
PEARSON (r) AND SPEARMAN'S (ρ) CORRELATION COEFFICIENTS BETWEEN THE EXTRACTED DESCRIPTORS AND BOTH SOIL WATER INDEX AND INTERPOLATED NDVI FOR UAVSAR PM FLIGHTS

Descriptors	SWI		Int. NDVI		Descriptors	SWI		Int. NDVI	
	r	ρ	r	ρ		r	ρ	r	ρ
α	0.12	**0.32**	**0.57**	**0.56**	P_s^{Y4R}	0.19	0.21	-0.28	**-0.40**
H	0.13	0.16	**0.62**	**0.62**	P_d^{Y4R}	0.30	0.30	**0.36**	0.31
γ^0_{HH}	0.18	0.22	-0.13	-0.20	P_v^{Y4R}	**0.36**	0.35	0.04	-0.04
γ^0_{HV}	0.37	**0.39**	0.07	-0.02	P_s^{G4U1}	0.19	0.20	-0.29	**-0.40**
γ^0_{VV}	0.26	0.27	-0.27	**-0.33**	P_d^{G4U1}	0.31	0.31	**0.35**	0.30
$SPAN$	0.23	0.27	-0.20	**-0.28**	P_v^{G4U1}	**0.37**	**0.38**	0.07	-0.03
HH/VV	-0.38	-0.35	**0.60**	0.48	P_s^{G4U2}	0.19	0.20	-0.29	**-0.40**
P_s^{FD}	0.19	0.20	-0.29	**-0.40**	P_d^{G4U2}	0.31	0.31	**0.35**	0.30
P_d^{FD}	0.25	0.25	**0.37**	0.36	P_v^{G4U2}	**0.37**	**0.38**	0.06	-0.03
P_v^{FD}	**0.37**	**0.39**	0.07	-0.02	P_s^{FDG}	0.19	0.21	-0.28	**-0.40**
P_s^{NNED}	0.19	0.21	-0.28	**-0.40**	P_d^{FDG}	0.25	0.24	**0.36**	0.35
P_d^{NNED}	0.25	0.24	**0.36**	0.35	P_v^{FDG}	**0.37**	**0.39**	0.07	-0.02
P_v^{NNED}	**0.37**	**0.39**	0.07	-0.02					

improves the correlation, whereas the information about moisture is almost uniquely brought by the double-bounce power.

f) PM Flights: Table XV reports the Pearson (r) and Spearman's (ρ) correlation coefficients calculated between both total and polarimetric descriptors and both SWI and interpolated NDVI for the PM flights. The highest correlation values are highlighted in gray and bold.

The results show that the correlation remains low for all the six model-based decomposition powers and the total descriptors, so it is difficult to find a proper relationship both with the SWI and the interpolated NDVI. However, the H/α decomposition shows that both the alpha angle and the entropy are sensitive to the vegetation variations (0.57, 0.62), while the correlation with the SWI is poor. The two linear regression models described by (2) and (3) were also applied to the PM flights for estimating SWI. In (3), the three contributions from the G4U1 were exploited since it was the decomposition in which the double-bounce and volume contributions showed the highest linear correlation with SWI. Fig. 14 shows the results of this exercise for the case in which the three decomposition powers (dB) and the three gamma-naught terms (dB) were used. Table XVI summarizes the results by considering all the decomposition powers and gamma-naught combinations: the Pearson linear correlation (r), the p-value, and the RMSE values between estimated and measured SWI are reported.

The exercise suggests that the best result is achieved when the three gamma-naught terms (γ^0_{HH}, γ^0_{HV}, γ^0_{VV}) are exploited ($r = 0.75, p < 0.01, \mathrm{RMSE} = 10.25\%$). It can be noted that the afternoon acquisitions exhibit generally worse performance with respect to the morning ones, a result that is generally expected. In fact, there is theoretical evidence of differences between morning and afternoon soil moisture retrievals. As for passive microwave radiometer, for instance, isothermal conditions found at the near-surface during early morning aid in the retrieval of surface soil moisture. The impact of the ionosphere at L-band is also expected to be minimized at night. The Soil Water Index was found only weakly dependent on the time of the day, but however within its coarse resolution area it is expected that the surface conditions are much more heterogeneous in the afternoon and the correlation between airborne data and SWI be lower, as in fact was observed in our analysis.

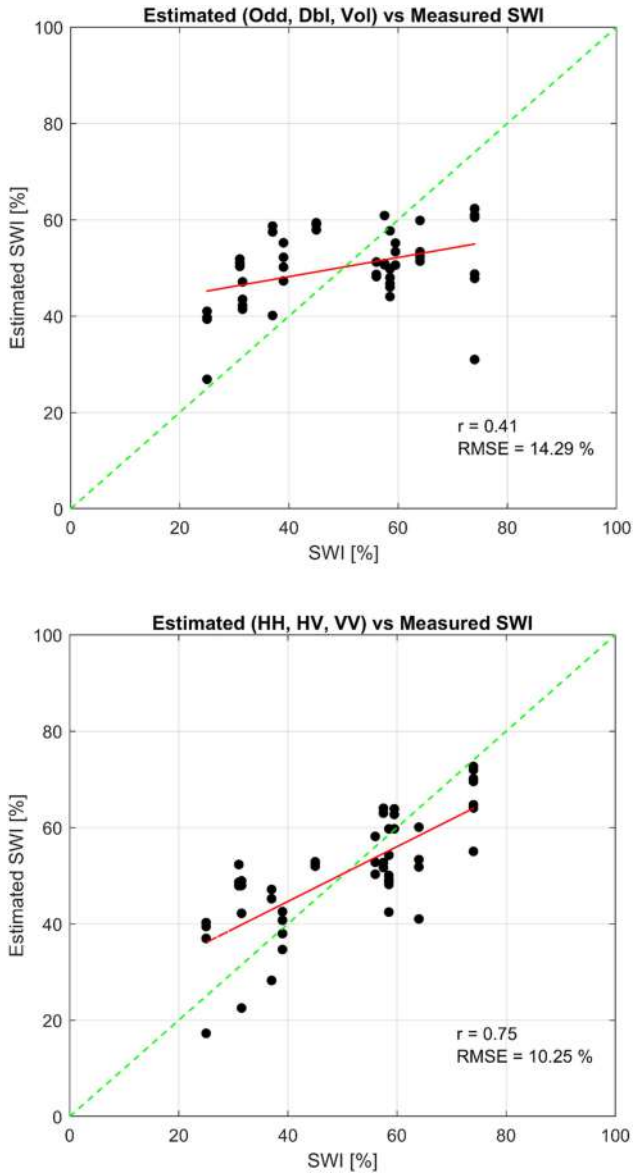

Fig. 14. Results of the two linear regression models applied to the PM flights (estimated versus measured SWI). The red line represents the best fit, while the green line is the best agreement between the data. Top: results obtained by considering the surface (Odd), double-bounce (Dbl), and volume (Vol) powers (dB) from the G4U1. Bottom: results obtained by considering the gamma-naught at HH, HV, VV polarizations. The Pearson linear correlation (r), and the RMSE are also displayed.

C. Monte Buey Site: 2019–2020 CONAE Field Campaign

The analysis was performed on five corn fields. The study was conducted by considering the correlation with both in-situ

TABLE XVI
RESULTS OF A LINEAR REGRESSION MODEL FOR ESTIMATING THE SOIL WATER INDEX FOR THE PM FLIGHTS BY CONSIDERING A COMBINATION OF THE G4U1 DECOMPOSITION POWERS AND A COMBINATION OF THE MEASURED BACKSCATTERING COEFFICIENTS

Input	r	p	$RMSE$ (%)
P_s^{G4U1}	0.19	1.9851e-01	15.33
P_d^{G4U1}	0.31	3.0134e-02	14.83
P_s^{G4U1}, P_d^{G4U1}	0.32	2.7057e-02	14.80
P_s^{G4U1}, P_d^{G4U1}, P_v^{G4U1}	**0.41**	**3.4781e-03**	**14.29**
γ_{HH}^0	0.18	2.2295e-01	15.35
γ_{HV}^0	0.37	8.7405e-03	14.49
γ_{VV}^0	0.26	7.4199e-02	15.07
γ_{HH}^0, γ_{HV}^0	0.50	2.2418e-04	13.52
γ_{HH}^0, γ_{VV}^0	0.40	4.5977e-03	14.31
γ_{HV}^0, γ_{VV}^0	0.38	7.0212e-03	14.44
γ_{HH}^0, γ_{HV}^0, γ_{VV}^0	**0.75**	**4.1108e-10**	**10.25**

data (i.e., soil moisture and plant height) and satellite derived target parameters (i.e., NDVI). We also recall that, contrarily to SMAPVEX 2012 and Yucatan Lake, the multipolarization backscattering coefficient sigma-naught was used instead of the gamma-naught. For this site, all considered fields fall within a narrow range of incidence angle values. Moreover, it is worth pointing out that in Argentina the plant residuals are not removed after the harvest and then the fields marked as fallow are not really bare soils. Table XVII reports the Pearson (r) and Spearman's (ρ) correlation coefficients calculated between both total and polarimetric descriptors and soil moisture, interpolated NDVI and plant height for the five corn fields of the Monte Buey site. The highest correlation values are highlighted in gray and bold.

First of all, we observe that the correlation analysis based on NDVI and in-situ plant height leads to very similar conclusions as the correlations match extremely well (correlation is equal to 0.99), although the use of plant height generates overall larger absolute correlation values. Then, the conclusions for the Monte Buey site can be considered reliable in terms of vegetation effects. Regarding the correlation with in-situ soil moisture, the backscattering coefficient exhibits a moderate linear correlation (r) with the measured soil moisture (0.48 for HH, 0.55 for HV, and 0.54 for VV); this correlation increases, especially for HV, if the Spearman's values are considered. The surface power from the six model-based decompositions is, in general, the descriptor with the lower linear correlation with respect to soil moisture (0.02–0.34); the double-bounce and, surprisingly, the volume powers are the polarimetric descriptors mostly correlated with soil moisture. While the former result has been already justified by the contribution of the soil in the dihedral scattering, the latter requires a deeper investigation. This result was also observed for the Yucatan Lake dataset and, again, it could be due to the amount of water contained in the canopy with a direct influence on the backscatter at HV polarization, from which the volume contribution is basically derived, also considering that in this case HV is the polarization with higher linear correlation values

TABLE XVII
PEARSON (r) AND SPEARMAN'S (ρ) CORRELATION COEFFICIENTS BETWEEN THE EXTRACTED DESCRIPTORS AND SOIL MOISTURE, INTERPOLATED NDVI, AND PLANT HEIGHT FOR THE CORN FIELDS IN MONTE BUEY

Descriptors	SM		Int. NDVI		PH	
	r	ρ	r	ρ	r	ρ
α	0.47	**0.64**	**0.74**	0.49	**0.94**	0.31
H	**0.42**	0.39	**0.73**	0.54	**0.85**	0.20
σ_{HH}^0	0.48	**0.59**	**0.54**	0.36	**0.82**	0.72
σ_{HV}^0	0.55	**0.69**	**0.69**	0.41	**0.95**	0.70
σ_{VV}^0	0.54	**0.59**	**0.41**	0.19	**0.69**	0.55
$SPAN$	0.52	**0.61**	**0.51**	0.32	**0.80**	0.67
HH/VV	0.16	**0.21**	0.58	**0.60**	**0.71**	0.46
P_s^{FD}	0.08	0.10	-0.02	0.02	-0.10	0.12
P_d^{FD}	0.46	**0.68**	**0.67**	0.42	**0.95**	0.68
P_v^{FD}	0.54	**0.70**	**0.68**	0.42	**0.95**	0.68
P_s^{NNED}	0.03	0.01	-0.03	-0.01	-0.14	0.11
P_d^{NNED}	0.46	**0.69**	**0.67**	0.42	**0.95**	0.68
P_v^{NNED}	0.54	**0.68**	**0.69**	0.39	**0.94**	0.69
P_s^{Y4R}	0.30	**0.38**	0.18	0.06	0.24	**0.33**
P_d^{Y4R}	0.47	**0.70**	**0.67**	0.42	**0.95**	0.66
P_v^{Y4R}	0.52	**0.68**	**0.64**	0.41	**0.94**	0.68
P_s^{G4U1}	0.17	0.19	0.06	0.03	0.03	**0.23**
P_d^{G4U1}	0.47	**0.68**	**0.68**	0.42	**0.95**	0.68
P_v^{G4U1}	0.53	**0.68**	**0.68**	0.40	**0.95**	0.72
P_s^{G4U2}	0.34	**0.43**	0.18	0.03	0.26	**0.33**
P_d^{G4U2}	0.47	**0.68**	**0.68**	0.42	**0.95**	0.68
P_v^{G4U2}	0.53	**0.68**	**0.70**	0.41	**0.95**	0.71
P_s^{FDG}	0.02	0.01	-0.05	-0.02	-0.16	0.10
P_d^{FDG}	0.48	**0.64**	**0.71**	0.41	**0.95**	0.68
P_v^{FDG}	0.55	**0.69**	**0.69**	0.41	**0.95**	0.70

with respect to soil moisture (0.55). Whether this result is due to a "cross-talk" effect between the three scattering contributions requires further investigation; the polarimetric calibration accuracy of the radar could be also a detrimental factor in the application of polarimetric decompositions. It is noticeable that, except for entropy, the Spearman's correlation values are higher with respect to those obtained involving the Pearson's correlation, likely due to the fact that a nonlinear relationship exists between the descriptors and soil moisture. The correlation of the surface term with NDVI and plant height is also low, as expected. The correlation between the power of the surface terms and both NDVI and plant height is not appreciable, so that the impact of the attenuation in this case is not appreciable. The double-bounce and volume powers from the six model-based decompositions along with the backscattering coefficient σ_{HV}^0, the entropy and the alpha angle are the descriptors that exhibit the higher linear correlation with the plant height and NDVI. As expected, even the backscattering coefficient σ_{HH}^0 has a large linear correlation with the measured plant height (0.82). The large correlation of entropy and the alpha angle with NDVI and plant height is an expected result, confirming the outcome of the corn

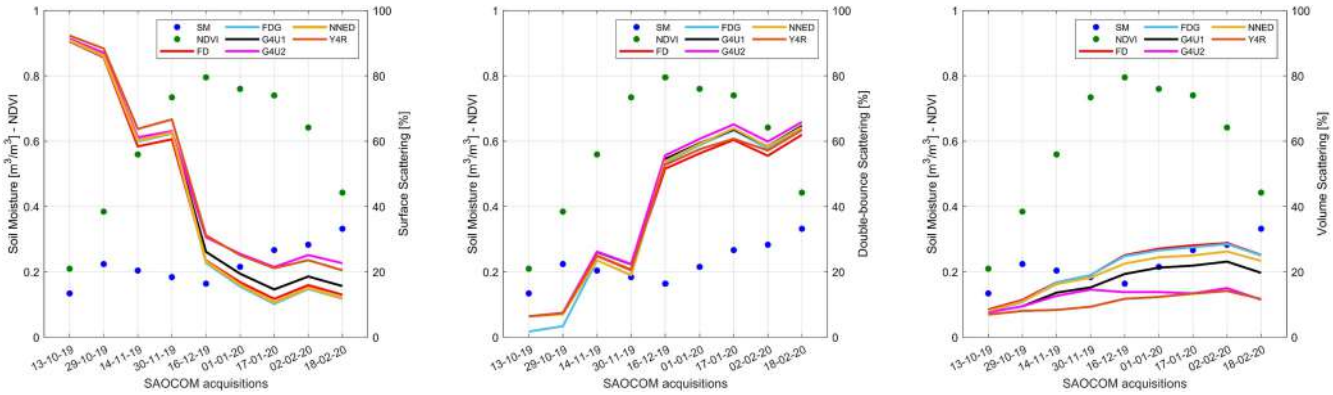

Fig. 15. Temporal evolution of the mean percentage of surface (left), double-bounce (middle), and volume contributions (right) for the six model-based decompositions (FD, FDG, G4U1, G4U2, NNED, Y4R). Soil moisture and NDVI are also reported in blue and green, respectively.

TABLE XVIII
RESULTS OF A LINEAR REGRESSION MODEL FOR ESTIMATING THE SOIL MOISTURE FOR THE CORN FIELDS IN THE MONTE BUEY SITE BY CONSIDERING A COMBINATIONS OF THE G4U2 DECOMPOSITION POWERS AND A COMBINATION OF THE MEASURED BACKSCATTERING COEFFICIENTS

Input	r	p	$RMSE$ (%)
P_s^{G4U2}	0.34	1.0725e-01	6
P_d^{G4U2}	0.47	2.0539e-02	6
P_s^{G4U2}, P_d^{G4U2}	0.51	1.1454e-02	6
$\boldsymbol{P_s^{G4U2}, P_d^{G4U2}, P_v^{G4U2}}$	**0.64**	**7.8098e-04**	**5**
σ_{HH}^0	0.48	1.7284e-02	6
σ_{HV}^0	0.55	5.7905e-03	6
σ_{VV}^0	0.54	6.2318e-03	6
σ_{HH}^0, σ_{HV}^0	0.55	5.8185e-03	6
σ_{HH}^0, σ_{VV}^0	0.55	5.5842e-03	6
σ_{HV}^0, σ_{VV}^0	0.57	3.3507e-03	5
$\boldsymbol{\sigma_{HH}^0, \sigma_{HV}^0, \sigma_{VV}^0}$	**0.64**	**6.9621e-04**	**5**

fields in SMAPVEX 2012. Indeed, the entropy is an indicator of the growth of the vegetation: when the vegetation increases, the target randomness increases as well and, consequently, the entropy becomes higher. Fig. 15 reports the temporal trend (i.e., average over different fields) of the mean percentage of surface, double-bounce, and volume powers, calculated with respect to the SPAN, for the six model-based decompositions. The spatial means of soil moisture (m^3/m^3) measurements and NDVI are also reported; they were previously linearly interpolated to fill the dates where soil moisture and NDVI were not collected and to ease the interpretation, highlighting the full temporal trend. It can be observed that the variable with the larger influence on the temporal evolution of the three scattering mechanisms is the NDVI, rather than the soil moisture, which has however a small dynamic range (plants are not irrigated and no relevant precipitation events were observed just before a SAOCOM acquisition). Note that, although NDVI decreases in January due to loss of chlorophyll, the plants were still at the maximum growing stage in that period. When the NDVI values are below 0.4, the surface is the predominant scattering mechanism. When the NDVI starts to increase, the double-bounce, and volume terms increase as well, whereas the surface power percentage progressively decreases as a consequence of the attenuation introduced by the growing vegetation. The trend is similar, but much more pronounced than in SMAPVEX 2012; indeed, in Monte Buey during the first SAR acquisition the plants were still very small (10 cm high or even fallow), and the temporal plot spans a longer temporal interval of the plant growing cycle (compare Figs. 7 and 15). It is observed that the volume percentage slightly increases with NDVI and plant growth (about 250 cm during the last SAOCOM acquisition) reaching a level of saturation over time (as also observed for the corn and soybean fields of SMAPVEX 2012), while the double-bounce progressively becomes the predominant scattering mechanism. The two linear regression models described by (2) and (3) were applied to retrieve soil moisture by considering alternatively as predictors a combination of the backscattering coefficients sigma-naught or the polarimetric surface (Odd), double-bounce (Dbl), and volume (volume) powers obtained by applying the G4U2. This decomposition was the one with generally the highest linear correlation with respect to the measured soil moisture. Fig. 16 shows the results of this exercise for the case in which the three decomposition powers (dB) and the three sigma-naught terms (dB) were used. Table XVIII summarizes the results by considering all the decomposition powers and sigma-naught combinations: the Pearson linear correlation (r), the p-value, and the RMSE values between estimated and measured soil moisture are reported.

The results obtained with the three sigma-naught coefficients are almost equal to the results given by the three G4U2 polarimetric powers ($r = 0.64$, $p < 0.01$, RMSE $= 5\%$). Considering three descriptors, i.e., a full-polarimetric radar, always improves the results, both for the total and polarimetric descriptors.

V. CONCLUSION

In this paper, seven polarimetric decompositions [Freeman-Durden three-components decomposition (FD), Yamaguchi four-components decomposition (Y4R), Singh four-components decomposition with/without extended volume scattering model (G4U2/G4U1), the Nonnegative Eigenvalue

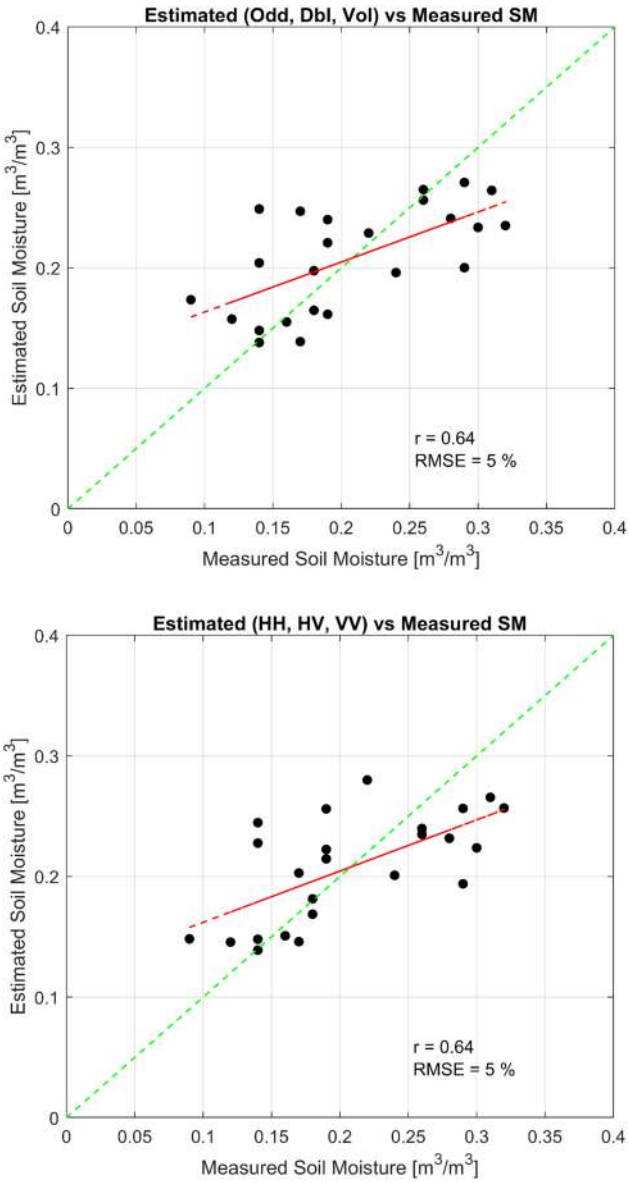

Fig. 16. Results of the two linear regression models applied to five corn fields in Monte Buey (estimated versus measured SM). The red line represents the best fit, while the green line is the best agreement between the data. Top: results obtained by considering the surface (Odd), double-bounce (Dbl), and volume (Vol) powers (dB) from the G4U2. Bottom: results obtained by considering the sigma-naught at HH, HV, VV polarizations. The Pearson linear correlation (r), and the RMSE are also displayed.

Decomposition (NNED), the Generalized Freeman-Durden decomposition (FDG), and the H\α decomposition] were applied to the polarimetric covariance or coherency matrices (C3/T3) derived from three L-band quad-polarimetric SAR datasets over three different agricultural areas across a latitudinal gradient. The goal of the study was to evaluate the sensitivity of polarimetric decompositions to soil and vegetation properties as compared to a combination of the backscattering coefficients (i.e., the elements of the main diagonal of the C3 matrices). The study also aimed to investigate which decomposition behaves best in view of a future exploitation within a soil moisture retrieval algorithm. Results revealed that there were not significant differences among sensitivities of the different decompositions tested in this study, even if their performances, in terms of correlation to soil moisture and vegetation, depend both on the crop type and the selected area of interest. To support this conclusion, in addition to the correlation analysis that was performed between the polarimetric descriptors and the in-situ variables, we have computed the Pearson linear correlation coefficient between all possible pairs of scattering mechanisms extracted after applying the different polarimetric decompositions. We found that the Pearson correlation coefficients were consistently very high (0.96 on average for the surface power, 1.00 on average for the double-bounce power, and 0.98 on average for the volume power). This supports the argument that choosing a particular decomposition versus another does not have a significant impact on the results. A main finding of the work is that, although the decompositions have revealed to be effective in distinguishing the different scattering mechanisms, those mechanisms are not unequivocally related to the bio-geophysical parameters of interest, namely soil moisture and vegetation biomass or other vegetation parameters (e.g., plant height and satellite-derived NDVI). In detail, the double-bounce is both affected by the reflection from the soil and that of the vertical stems of the plants. Therefore, depending on the type of crops, the sensitivity to soil moisture (e.g., the case of wheat plants where scattering is weak and attenuation is the main effect) or the sensitivity to plant growth (e.g., the case of corn with bigger and higher vertical stems) can be emphasized. Even the surface term is affected by the vegetation; it is decreased by the increase of attenuation as the vegetation grows, thus exhibiting in some cases a non-negligible negative correlation with biomass. A positive correlation between the volume component and the soil moisture was also observed. This can be explained by the process of absorption of the soil water by the vegetation (the osmosis process) that makes the vegetation water content increase when the soil becomes wetter. It is known that the water in the vegetation strongly affects the absorption and scattering properties of the volume. Another effect can be due to the interception of water by the vegetation after precipitation or irrigation events. This water does not necessarily contribute to soil moisture and runoff, but certainly affects the scattering properties of the volume. By comparing a multivariate linear best fitting using alternatively the three multipolarization backscatter coefficients and the power of the three scattering mechanisms derived from the six model-based polarimetric decompositions, the results suggested that the estimates are generally comparable in terms of Pearson linear correlation and RMSE, except for the UAVSAR PM flights, for which the use of the total backscattering coefficients gamma-naught returned the best results. We recall that this conclusion has been drawn based on the analysis of three different datasets, including both airborne and satellite SAR data, different flight altitudes and incidence angles, as well as different sites, vegetation types, and reference data (in-situ as well as satellite derived bio-geophysical data). The two linear models involved in this study for estimating soil moisture or Soil Water Index were very simple models aiming to compare the performances of different sets of input features rather

than representing an ultimate retrieval approach. They can be refined when analyzing new datasets to include incidence angle when required. It is undoubted and largely demonstrated that polarimetric radar is a powerful tool for remote sensing the Earth surface. Exploiting the fully polarimetric information, which implies not only the multipolarized scattered power but also the complex covariance between the elements of the scattering matrix, can be very effective. However, the tested polarimetric decompositions aimed to discriminate scattering mechanisms have been found not as much effective in isolating specific bio-geophysical parameters of interest, such as soil moisture.

Acknowledgment

The authors would like to thank the NASA Jet Propulsion Laboratory for providing the UAVSAR data and the SMAPVEX 2012 team for sharing the in-situ measurements collected during the field experiment. The authors are also grateful to the Argentinian Space Agency for the SAOCOM-1A acquisitions and the ground data acquired during the 2019-2020 field campaign. Some of the polarimetric SAR decompositions were applied by using the PolSARpro 6.0 Biomass Edition software, for which the authors would like to thank the development team and ESA for making it available.

References

[1] N. Baghdadi, M. El Hajj, M. Zribi, and S. Bousbih, "Calibration of the water cloud model at c-band for winter crop fields and grasslands," *Remote Sens.*, vol. 9, 2017, Art. no. 969, doi: 10.3390/rs9090969.

[2] M. A. Acuña, F. Fascetti, P. Ferrazzoli, L. Guerriero, and N. Pierdicca, "Modelling L band backscattering of wheat in Argentinean Pampas and its application to soil moisture retrieval," *Int. J. Remote Sens.*, vol. 41, no. 14, pp. 5083–5102, 2020, doi: 10.1080/01431161.2020.1727050.

[3] H. Lievens and N. E. C. Verhoest, "On the retrieval of soil moisture in wheat fields from L-band SAR based on water cloud modeling, the IEM, and effective roughness parameters," *IEEE Geosci. Remote Sens. Lett.*, vol. 8, no. 4, pp. 740–744, Jul. 2011, doi: 10.1109/LGRS.2011.2106109.

[4] I. Hajnsek, T. Jagdhuber, H. Schon, and K. P. Papathanassiou, "Potential of estimating soil moisture under vegetation cover by means of PolSAR," *IEEE Trans. Geosci. Remote Sens.*, vol. 47, no. 2, pp. 442–454, Feb. 2009, doi: 10.1109/TGRS.2008.2009642.

[5] H. Wang, R. Magagi, and K. Goita, "Comparison of different polarimetric decompositions for soil moisture retrieval over vegetation covered agricultural area," *Remote Sens. Environ.*, vol. 199, pp. 120–136, 2017, doi: 10.1016/j.rse.2017.07.008.

[6] T. Jagdhuber, I. Hajnsek, and K. P. Papathanassiou, "An iterative generalized hybrid decomposition for soil moisture retrieval under vegetation cover using fully polarimetric SAR," *IEEE J. Sel. Topics Appl. Earth Observ. Remote Sens.*, vol. 8, no. 8, pp. 3911–3922, Aug. 2015, doi: 10.1109/JSTARS.2014.2371468.

[7] T. Jagdhuber, I. Hajnsek, A. Bronstert, and K. P. Papathanassiou, "Soil moisture estimation under low vegetation cover using a multi-angular polarimetric decomposition," *IEEE Trans. Geosci. Remote Sens.*, vol. 51, no. 4, pp. 2201–2215, Apr. 2013, doi: 10.1109/TGRS.2012.2209433.

[8] A. Freeman and S. L. Durden, "A three-component scattering model for polarimetric SAR data," *IEEE Trans. Geosci. Remote Sens.*, vol. 36, no. 3, pp. 963–973, May 1998, doi: 10.1109/36.673687.

[9] Y. Yamaguchi, A. Sato, W. Boerner, R. Sato, and H. Yamada, "Four-component scattering power decomposition with rotation of coherency matrix," *IEEE Trans. Geosci. Remote Sens.*, vol. 49, no. 6, pp. 2251–2258, Jun. 2011, doi: 10.1109/TGRS.2010.2099124.

[10] G. Singh, Y. Yamaguchi, and S. Park, "General four-component scattering power decomposition with unitary transformation of coherency matrix," *IEEE Trans. Geosci. Remote Sens.*, vol. 51, no. 5, pp. 3014–3022, May 2013, doi: 10.1109/TGRS.2012.2212446.

[11] J. J. van Zyl, M. Arii, and Y. Kim, "Model-based decomposition of polarimetric SAR covariance matrices constrained for nonnegative eigenvalues," *IEEE Trans. Geosci. Remote Sens.*, vol. 49, no. 9, pp. 3452–3459, Sep. 2011, doi: 10.1109/TGRS.2011.2128325.

[12] S. R. Cloude, "Decomposition theorems," in *Polarisation: Applications in Remote Sensing*, 1st ed. London, U.K.: Oxford Univ. Press, 2010, pp. 198–201.

[13] S. R. Cloude and E. Pottier, "A review of target decomposition theorems in radar polarimetry," *IEEE Trans. Geosci. Remote Sens.*, vol. 34, no. 2, pp. 498–518, Mar. 1996, doi: 10.1109/36.485127.

[14] J. Van Zyl and Y. Kim, "Advanced polarimetric concepts," in *Synthetic Aperture Radar Polarimetry*. Hoboken, NJ, USA: Wiley, 2011, pp. 76–87.

[15] H. McNairn et al., "The soil moisture active passive validation experiment 2012 (SMAPVEX12): Prelaunch calibration and validation of the SMAP soil moisture algorithms," *IEEE Trans. Geosci. Remote Sens.*, vol. 53, no. 5, pp. 2784–2801, May 2015, doi: 10.1109/TGRS.2014.2364913.

[16] NISAR UAVSAR AM-PM Campaign Deployment (L-band) website. [Online]. Available: uavsar.jpl.nasa.gov/cgi-bin/deployment.pl?id=L20190606

[17] SMAPVEX12 website. [Online]. Available: http://smapvex12.espaceweb.usherbrooke.ca/

[18] UAVSAR website. [Online]. Available: uavsar.jpl.nasa.gov

[19] SAOCOM-1 Level 1 Products Format documentation. [Online]. Available: catalogos.conae.gov.ar/catalogo/catalogoSatSaocomDocs.html

[20] Soil Water Index. [Online]. Available: land.copernicus.eu/global/products/swi

[21] Soil Water Index Product User Manual. [Online]. Available: land.copernicus.eu/global/products/swi

[22] J. A. Richards, "The technology of radar imaging," in *Remote Sensing With Imaging Radar*. Berlin, Germany: Springer, 2009, pp. 81–89.

[23] Y. Yamaguchi, T. Moriyama, M. Ishido, and H. Yamada, "Four-component scattering model for polarimetric SAR image decomposition," *IEEE Trans. Geosci. Remote Sens.*, vol. 43, no. 8, pp. 1699–1706, Aug. 2005, doi: 10.1109/TGRS.2005.852084.

[24] G. H. X. Shiroma, M. Lavalle, and S. M. Buckley, "An area-based projection algorithm for SAR radiometric terrain correction and geocoding," *IEEE Trans. Geosci. Remote Sens.*, vol. 60, 2022, Art. no. 5222723, doi: 10.1109/TGRS.2022.3147472.

[25] F. T. Ulaby, P. P. Batlivala, and M. C. Dobson, "Microwave backscatter dependence on surface roughness, soil moisture, and soil texture: Part I-bare soil," *IEEE Trans. Geosci. Electron.*, vol. 16, no. 4, pp. 286–295, Oct. 1978, doi: 10.1109/TGE.1978.294586.

[26] H. Shi et al., "Soil moisture retrieval over agricultural fields from L-band multi-incidence and multitemporal PolSAR observations using polarimetric decomposition techniques," *Remote Sens. Environ.*, vol. 261, 2021, Art. no. 112485, doi: 10.1016/j.rse.2021.112485.

[27] H. Wang, R. Magagi, K. Goita, T. Jagdhuber, and I. Hajnsek, "Evaluation of simplified polarimetric decomposition for soil moisture retrieval over vegetated agricultural fields," *Remote Sens.*, vol. 8, 2016, Art. no. 142, doi: 10.3390/rs8020142.

[28] M. El Hajj, N. Baghdadi, H. Bazzi, and M. Zribi, "Penetration analysis of SAR signals in the C and L bands for wheat, maize, and grasslands," *Remote Sens.*, vol. 11, 2019, Art. no. 31, doi: 10.3390/rs11010031.

[29] Y. Zhou, A. Sharma, M. Kurum, R. H. Lang, P. E. O'Neill, and M. H. Cosh, "The backscattering contribution of soybean pods at L-band," *Remote Sens. Environ.*, vol. 248, 2020, Art. no. 111977, doi: 10.1016/j.rse.2020.111977.

Giovanni Anconitano (Student Member, IEEE) received the M.Sc. degree in space and astronautical engineering in January 2019 from the Sapienza University of Rome, Rome, Italy, where he is currently working toward the Ph.D. degree in information and communication technology.

In 2020, he was a Research Collaborator with the Sapienza Aerospace Research Center, Rome, Italy. In 2021, he was a Research Fellow with the Department of Information Engineering, Electronics, and Telecommunications, Sapienza University of Rome. His research interests include the development of algorithms for soil moisture retrieval from satellite and airborne SAR data, SAR Polarimetry, correction of the vegetation effects on the radar response, and electromagnetic scattering models.

Marco Lavalle received the M.Sc. degree in telecommunication engineering from the University of Rome Tor Vergata, Rome, Italy, in 2006, and the Ph.D. degree in telecommunication engineering and geoinformation from the University of Rennes 1, Rennes, France and from the University of Rome Tor Vergata, in December 2009.

He is a Scientist and Group Supervisor with the NASA Jet Propulsion Laboratory, California Institute of Technology, Pasadena, California. From 2006 to 2008, he was Visiting Scientist with the European Space Agency where he supported ESA's activities on polarimetric radar calibration and polarimetric radar interferometric algorithm development. From January 2010 to December 2011, he was NASA Postdoctoral Fellow with the Jet Propulsion Laboratory (JPL), California Institute of Technology. He has been permanent scientist with the Radar Science and Engineering Section at JPL since January 2012. He was Principal Investigator and co-Investigator for several NASA programs. He is the lead for the 2020 NASA Distributed Aperture Radar Tomographic Sensors project, and member of the ESA ROSE-L, NISAR, and UAVSAR Project Science Teams. He is currently Group Supervisor for the SAR Algorithms and Processing Group at JPL. His research interests include retrieval algorithm development, physical and statistical model formulation, electromagnetic propagation, scattering theory, SAR tomography, polarimetric SAR interferometry, ecosystem modeling, and surface parameter estimation.

Dr. Lavalle is the recipient of the 2019 NASA Early Career Public Achievement Medal, the 2020 JPL Lew Allen Award for Excellence, and the Student Prize Paper Award at the EUSAR 2008 Conference (Friedrichshafen, Germany).

Mario Alberto Acuña received the B.Sc. and M.Sc. degrees in physics from the Balseiro Institute, Bariloche, Rio Negro, Argentina, in 2006 and 2008, respectively, and the Ph.D. degree in geoinformation from the Tor Vergata University of Rome, Rome, Italy, in 2020 with a thesis titled "SAR Signature Modeling of the Pampas Region main crops".

He has been working at the Argentine Space Agency "CONAE" for over 10 years, with a focus on this topic and several publications.

Nazzareno Pierdicca (Senior Member, IEEE) received the Laurea (Doctor's) degree (*cum laude*) in electronic engineering from the Sapienza University of Rome, Rome, Italy, in 1981.

In 1978–1982, he was with the Italian Agency for Alternative Energy. From 1982 to 1990, he was with the Remote Sensing Division of Telespazio, Rome, Italy. In 1990, he joined the Department of Information Engineering, Electronics and Telecommunications, Sapienza University of Rome. He is currently a Full Professor and teaches remote sensing and electromagnetic fields with the Faculty of Engineering, Sapienza University of Rome. His research interests include electromagnetic scattering and emission models for sea and bare soil surfaces and their inversion, microwave radiometry of the atmosphere, radar land applications, and GNSS reflectometry.

Dr. Pierdicca is a Senior member of IEEE Geoscience and Remote Sensing Society, past Chairman of the GRSS Central Italy Chapter, and chair of the GRSS Modeling in Remote Sensing Technical Committee.